AD-A110 838 SCRIPPS INSTITUTION OF OCEANOGRAPHY LA JOLLA CA CENT--ETC F/G 8/3
FLUID-SEDIMENT INTERACTIONS ON BEACHES AND SHELVES.(U)
SEP 81 D L INMAN, C D WINANT, R T GUZA N00014-75-C-0300
UNCLASSIFIED SIO-REF-81-27 NL

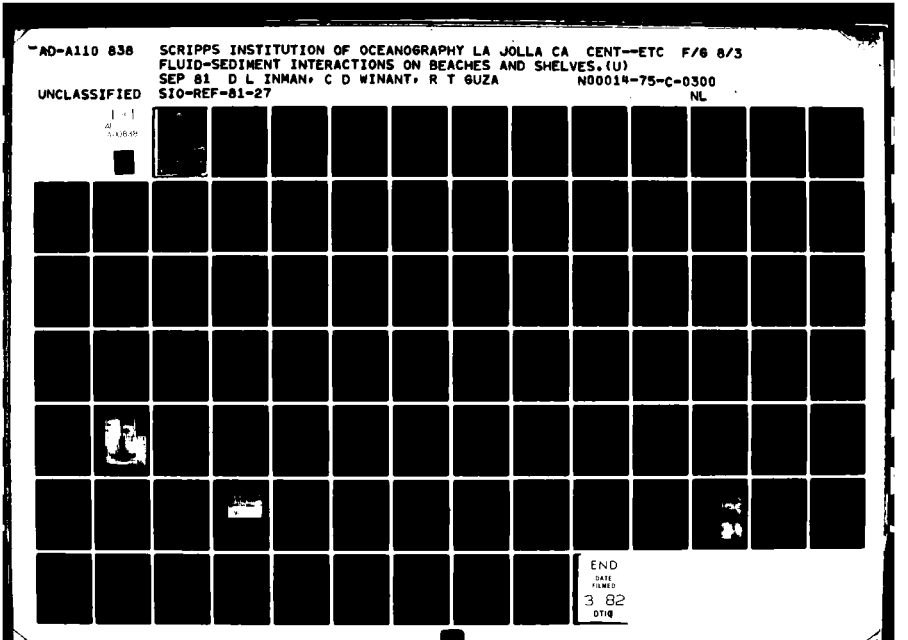

END
DATE FILMED
3 82
DTIC

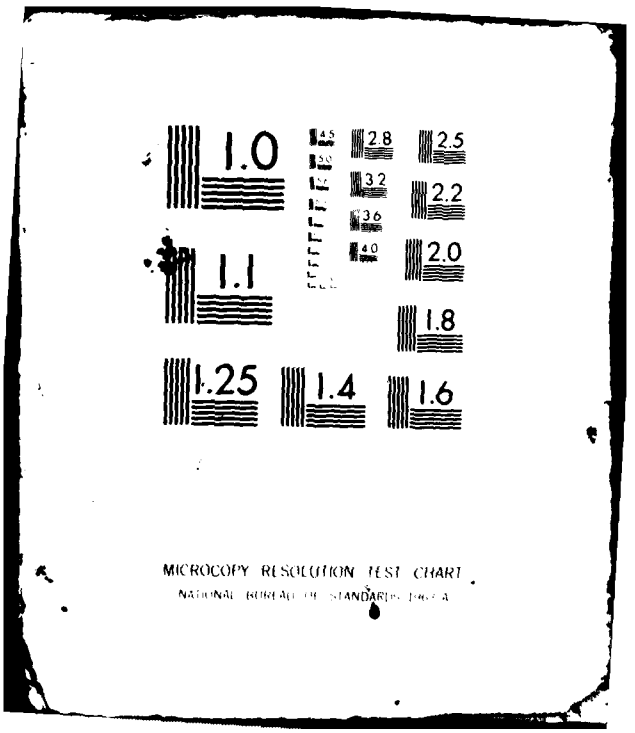
1.0
1.1
1.25
1.4
1.6
2.8
3.2
3.6
4.0
2.5
2.2
2.0
1.8
MICROCOPY RESOLUTION TEST CHART

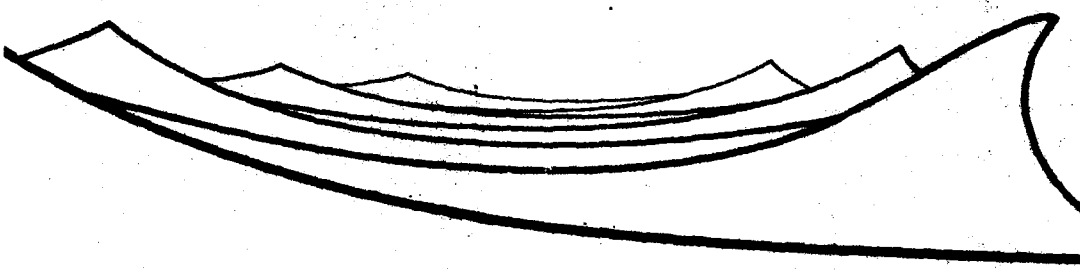

# SIO REFERENCE SERIES

## FLUID-SEDIMENT INTERACTIONS ON BEACHES AND SHELVES

## PROGRESS REPORT 1980 - 1981

D.L.Inman, R.T. Guza, C.D. Winant, R.E. Flick



SIO Reference 81 - 22 September 1981



University of Cali phy

SECURITY CLASSIFICATION OF THIS PAGE (When Data Entered)

## REPORT DOCUMENTATION PAGE

READ INSTRUCTIONS BEFORE COMPLETING FORM

1. REPORT NUMBER

2. GOVT ACCESSION NO. AD-A110 838

3. RECIPIENT'S CATALOG NUMBER

4. TITLE (and Subtitle)
FLUID-SEDIMENT INTERACTIONS ON BEACHES AND SHELVES

5. TYPE OF REPORT & PERIOD COVERED
Progress Report 1980-1981

6. PERFORMING ORG. REPORT NUMBER
SIO Reference Series 81-27

7. AUTHOR(s)
D.L.Inman R.T.Guza
C.D.Winant R.E.Flick

8. CONTRACT OR GRANT NUMBER(s)
N00014-75-C-0300

9. PERFORMING ORGANIZATION NAME AND ADDRESS
University of California, San Diego
Scripps Institution of Oceanography
Center for Coastal Studies
La Jolla, CA. 92093

10. PROGRAM ELEMENT, PROJECT, TASK AREA & WORK UNIT NUMBERS
Code 422 (Old 462)CS

11. CONTROLLING OFFICE NAME AND ADDRESS
Office of Naval Research, Coastal Sciences Prog.
Code 422 CS (Old 462)
Arlington, Virginia 22217

12. REPORT DATE
11 September 1981

13. NUMBER OF PAGES
86

14. MONITORING AGENCY NAME & ADDRESS (if different from Controlling Office)

15. SECURITY CLASS. (of this report)
Unclassified

15a. DECLASSIFICATION/DOWNGRADING SCHEDULE

16. DISTRIBUTION STATEMENT (of this Report)
Distribution unlimited



17. DISTRIBUTION STATEMENT (of the abstract entered in Block 20, if different from Report)



18. SUPPLEMENTARY NOTES

19. KEY WORDS (Continue on reverse side if necessary and identify by block number)

20. ABSTRACT (Continue on reverse side if necessary and identify by block number)

This research seeks to predict shelf and beach forms and their changes from knowledge of local bathymetry and the driving forces due to winds, waves and currents and their complicated interactions with nearshore sediments. The work falls into three distinct but interdependent areas of research: wave and current dynamics; fluid-sediment interactions; coastal zone remote sensing.

next page

DD FORM 1 JAN 73 1473 EDITION OF 1 NOV 65 IS OBSOLETE
S/N 0102-LF-014-6601

SECURITY CLASSIFICATION OF THIS PAGE (When Data Entered)

The principal area of interest in wave and current dynamics continues to be wind-generated, surface gravity waves and the currents and other fluid motions which derive their energy from surface waves. The fluid-sediment interaction studies lead to an understanding of the shelf and beach sediment response including the fundamental rheology of granular fluids, the longshore and on-offshore transport of sand and the formation of features like cusps and bars. The coastal zone remote sensing tasks are largely exploratory in nature, with the general objective of determining the extent to which signatures from remote sensors can be used to define the broader spatial characteristics of driving forces, and the larger scale ocean surface patterns that are characteristic of nearshore dynamics.

# FLUID-SEDIMENT INTERACTIONS ON BEACHES AND SHELVES

PROGRESS REPORT

1980 - 1981

Principal Investigators

D. L. Inman, R. T. Guza,
C. D. Winant, R. E. Flick

UCSD Proposal Number 2077

University of California, San Diego
Scripps Institution of Oceanography
Center for Coastal Studies
La Jolla, California 92093

Under Contract N00014-75-C-0300
Office of Naval Research, Coastal Sciences Program Code 462
Arlington, Virginia 22217

SIO Reference Series No. 81-27

August 198[illegible]

CONTENTS

## 1. PREFACE AND TIMETABLE

This report presents progress during the first year, and outlines modifications in the research plan of the second year of a three-year continuation of our ongoing research effort. This research seeks to predict shelf and beach forms and their changes from knowledge of local bathymetry and the driving forces due to winds, waves and currents and their complicated interactions with nearshore sediments. The full three-year effort was detailed in the proposal submitted last year.

Table 1 shows the research timetable proposed. There are no major changes in the planning. The following progress reports cover the individual tasks addressed in the 1980-81 contract year, as indicated by arrows.

## 2. GENERAL RESEARCH PLAN 1980 - 1983

The proposed work falls into three distinct but interdependent areas of research. They are:

A. Wave and current dynamics,

B. Fluid-sediment interactions,

C. Coastal zone remote sensing.

Each area logically divides into several "tasks" addressing specific scientific or instrumentation problems. These tasks are also interrelated, but vary in complexity and duration depending on the objectives. They will be phased in and out of the research program depending on the scientific merit and results, the interest of ONR and the interests and goals of

the principal investigators. The proposed tasks and their tentative timetables for the three year period 1980-1983 are shown in Table 1.

It is clear that the overall objective of the research program dictates the specific goals of the individual tasks. For example, waves and currents in nearshore waters are the driving forces for sediment motion, as well as being interesting and important in their own right. Progress on the prediction of shelf and beach topographic forms clearly requires improvements in the specification of fluid-driving forces. Fluid-sediment interactions are the cornerstone of this research project, and also pose the most difficult and complex set of problems. Even the most fundamental laws, the equations of motion, for granular fluids are not completely known, much less solved. The analogous laws for fluids have been known for hundreds of years. Approximations and empirical deductions, however, still allow progress to be made in many areas of fluid-sediment interaction. Frequently, fluid and fluid-sediment interaction experiments are run simultaneously, emphasizing the synergy between these objectives.

The objective of the remote sensing task is to use and refine existing techniques to study beaches and shelves, rather than to develop new remote sensing instrumentation. The opportunities for wide spatial coverage, without great time lags, of course makes remote sensing an attractive way of gathering data which would be prohibitively expensive to obtain using traditional "ground truth" sensors.

Table 1

FLUID-SEDIMENT INTERACTION ON BEACHES AND SHELVES

Research Timetable

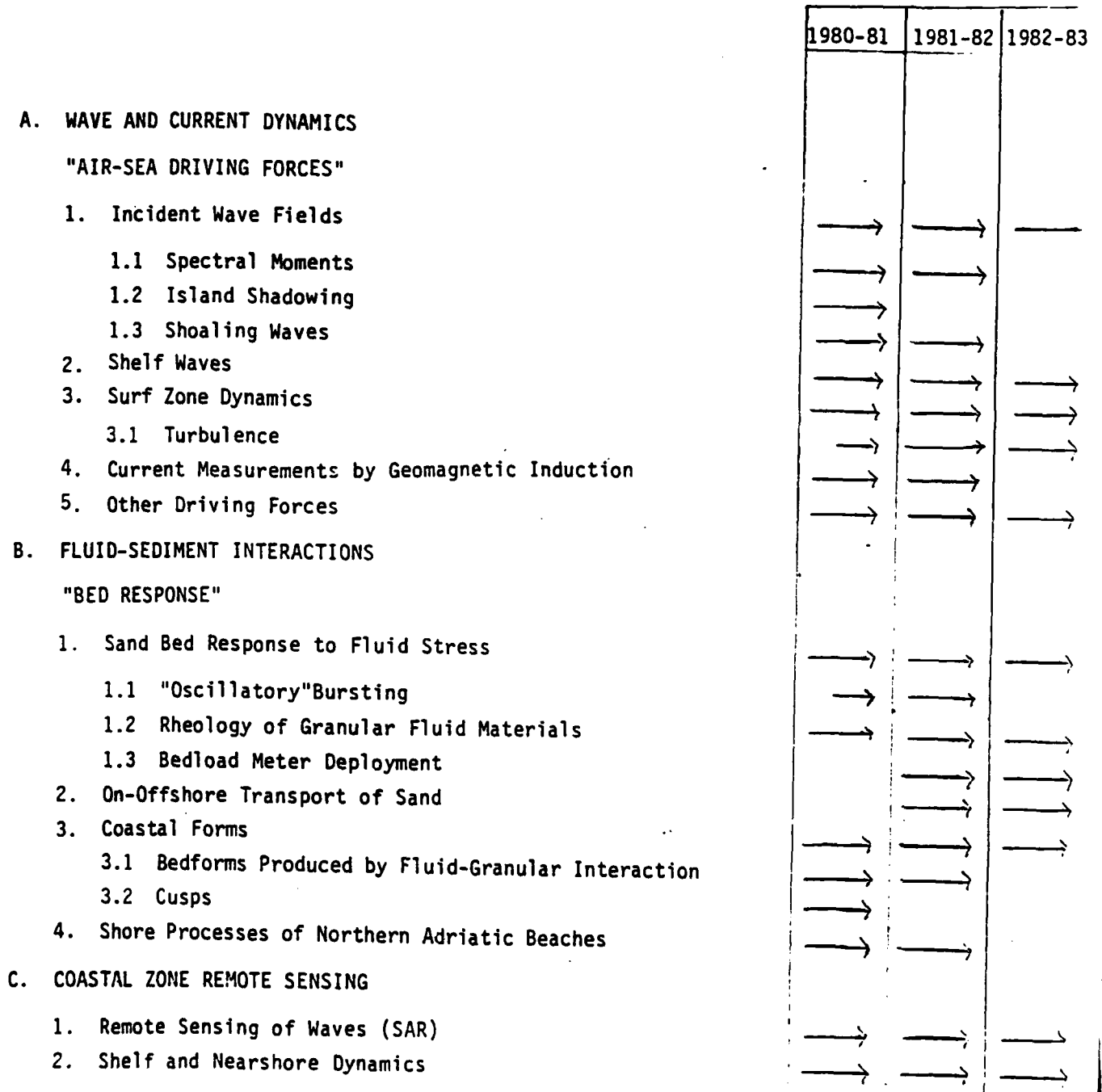

The underlying assumption behind this research project is that the dynamics of the shore and shelf areas of the world are governed by the same physical processes, although individual processes may differ in importance in specific areas thus producing the world's varied coastlines. Much of coastal research is directed toward the detailed description of specific areas and the treatment of these areas as unique entities. In contrast, this work seeks to understand these basic underlying physical processes so that the results may be applied to all coastal areas.

## A. WAVE AND CURRENT DYNAMICS

"AIR-SEA DRIVING FORCES"

The principal area of interest in the broad sense continues to be wind generated, surface gravity waves and currents and other fluid modes which derive their energy from these. Emphasis over the past year has been on: developing estimation techniques for momentum flux (Task A1.1); completion of the island shadowing project (A1.2); development and testing of a broadly applicable wave shoaling model (A1.3); an analysis of run-up and swash data at surf-beat frequencies (A2); preliminary work to measure the gross properties of turbulence in and near the surf zone (A3.1); and, in addition, instrument development has proceeded in preparation for measurements of the water flow-induced electric potential across the entrance of a tidal basin (A4).

The ultimate interest in studying the forcing functions is to understand their mechanics so that their full potential as driving forces may be applied to the study of fluid-sediment interactions and to sediment response. This is the guiding principle in selecting areas of study.

### A1. Incident Wave Fields

#### A1.1 Spectral Moments (S. S. Pawka)

The onshore flux of longshore directed wave momentum, $S_{yx}$, is an important forcing function for nearshore processes. $S_{yx}$ has been shown to drive the longshore current inside the surf zone (Bowen, 1969) and to be an important factor in the longshore transport of sand (e.g. Inman and Bagnold, 1963; Bailard and Inman, 1981). Coastal researchers have expended considerable effort in attempts to make accurate

measurements of this wave-field parameter. However, the statistical nature of these measurements has not been previously addressed.

$S_{yx}$ , expressed as a function of frequency, is related to the following moment of the frequency-directional spectrum, $E(f,\alpha)$,

$$S_{yx}(f) = n(f) \int_0^{2\pi} \cos\alpha \sin\alpha \, E(f,\alpha) \, d\alpha \qquad \text{(A1.1)}$$

where $\alpha$ is propagation direction, $f$ is the wave frequency, and $n(f)$ is the ratio of group to phase speed. Accurate estimates of $S_{yx}(f)$ can be computed from accurate measurements of $E(f,\alpha)$, say from a pressure sensor array, and integrating as in A1.1. In principle, <u>direct</u> estimates of the $S_{yx}$ moment can be made with a "slope array" (Seymour and Higgins, 1977) or a biaxial current meter (Pawka, in prep.). For example, the co-spectrum of the slopes, $\eta_x = \frac{\partial \eta}{\partial x}$ , $\eta_y = \frac{\partial \eta}{\partial y}$ obtained from the slope array has the form

$$C_{\eta_x \eta_y}(f) = k^2 \int_0^{2\pi} \cos\alpha \sin\alpha \, E(f,\alpha) \, d\alpha \qquad \text{(A1.2)}$$

These direct measurement techniques have two limitations. First, these "orthogonal component" systems have relatively poor resolution power for the definition of the directional spectrum $E(f,\alpha)$. The poor resolution would render these systems inadequate for the detailed study of the directional wave properties discussed in Section A1.2. Second, the (Gaussian) statistical nature of waves leads to a variance of an as yet undetermined form in the estimates of $S_{yx}$. These statistical variations and their effect on "$S_{yx}$ array" data applications are addressed in this task.

The probability density function for the co-spectrum in a 2-dimensional Gaussian random field was developed by Goodman (1957). Three

example density functions of this distribution family are shown in Figure A1-1. The effect of varying directional spectrum characteristics and sampling specifications on the shape of these distributions was studied. The dependence of distribution variance and skewness on the width of a unimodal directional peak and the degree of spectral averaging is shown in Figure A1-2. Both parameters strongly influence these low order distribution moments. Broad directional spectra increase the expected variability of $S_{yx}(f)$ estimates requiring longer sampling periods for stable measurements. Using the analytic density functions, appriori knowledge of the wave directional characteristics can be used in the design of sampling specifications of nearshore experiments or wave climatological measurement systems.

The variance of $S_{yx}(f)$ estimates is lowest for unidirectional wave conditions (Figure A1-3). Estimates of zero mean $S_{yx}(f)$ conditions may have relatively large absolute variances while this is not true for frequency spectrum estimates. The directional moments which determine the variance of $S_{yx}(f)$ estimates can all be directly measured with a biaxial current meter system. Therefore, this limited system not only yields an estimate of $S_{yx}(f)$ but also its expected variance.

A linear array of sensors can be used to estimate the wave directional spectra. The integration of these spectra (Equation A1.1) yields an estimate of $S_{yx}(f)$. The probability density functions discussed above are not strictly applicable to array measurements, which have some spatial averaging of the wave field. However, Pawka (in prep.) has demonstrated good comparison of linear array estimates of $S_{yx}(f)$ with those obtained from a slope array. These comparisons included close agreement

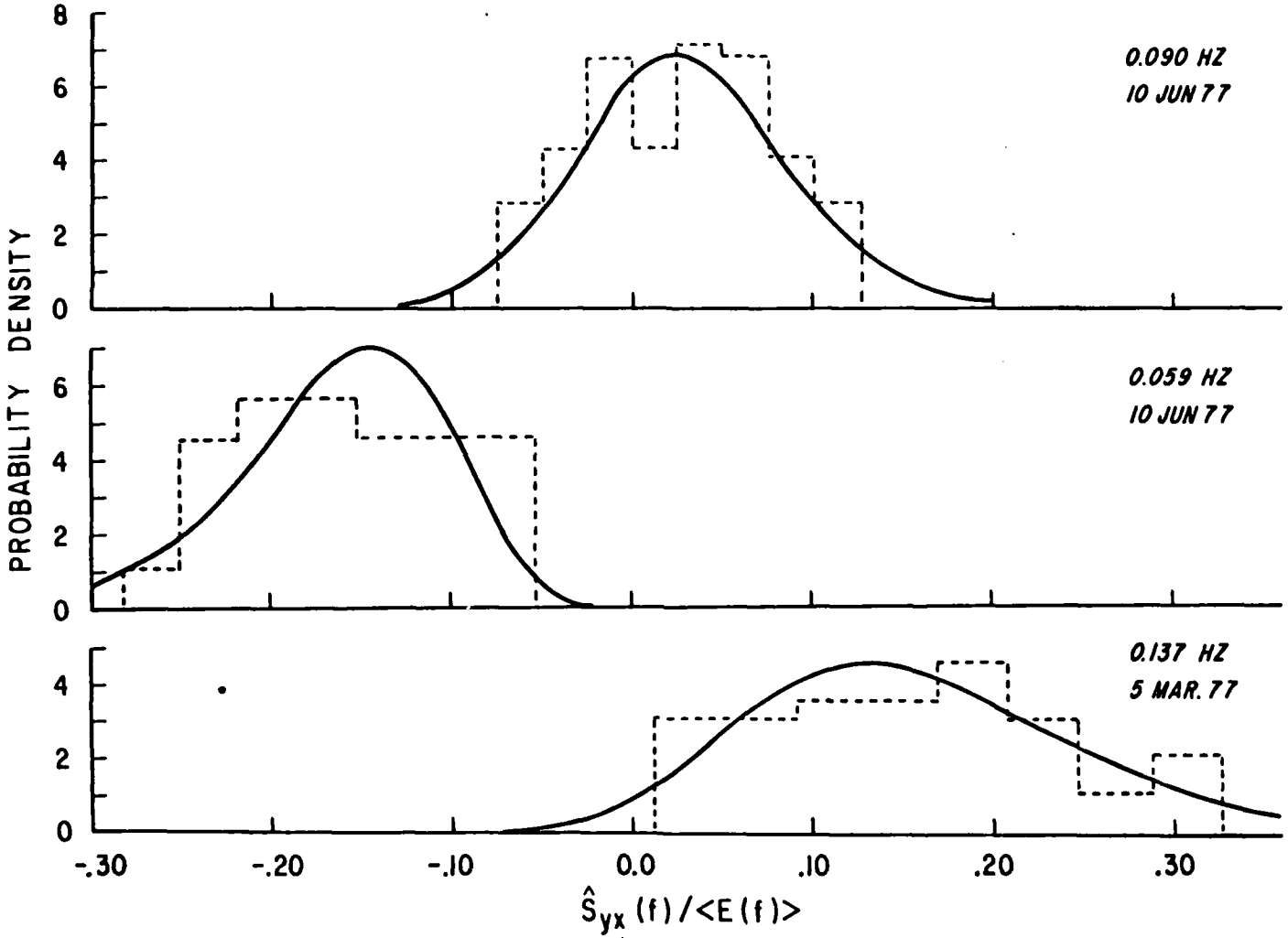


Figure A1-1. Comparisons of analytic density functions (solid line) with sample distributions of $S_{yx}(f)$ (dashed line). The sample distributions were obtained from a 1-2-4-5 configuration linear array (unit lag 33 m) in a mean water depth of 9.6 m by the integration of the directional spectrum (Equation A1.1).

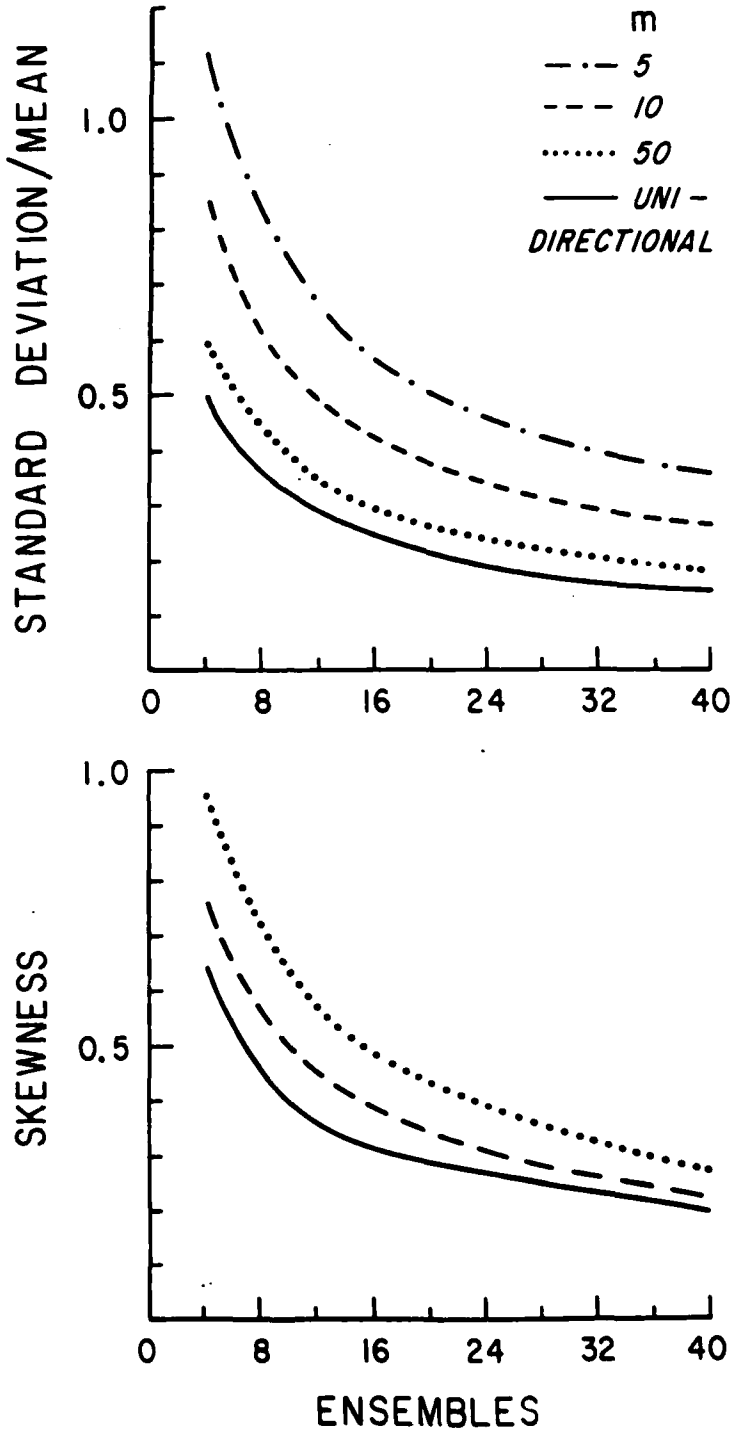


Figure A1-2. Dependence of normalized 2nd and 3rd order moments of $S_{yx}(f)$ distribution on the width of a unimodal directional spectrum and the number of ensembles averaged. The directional distribution employed was: $E(\alpha) = \cos^{m}(\alpha-10°)$ where $\alpha$ is the propagation direction.

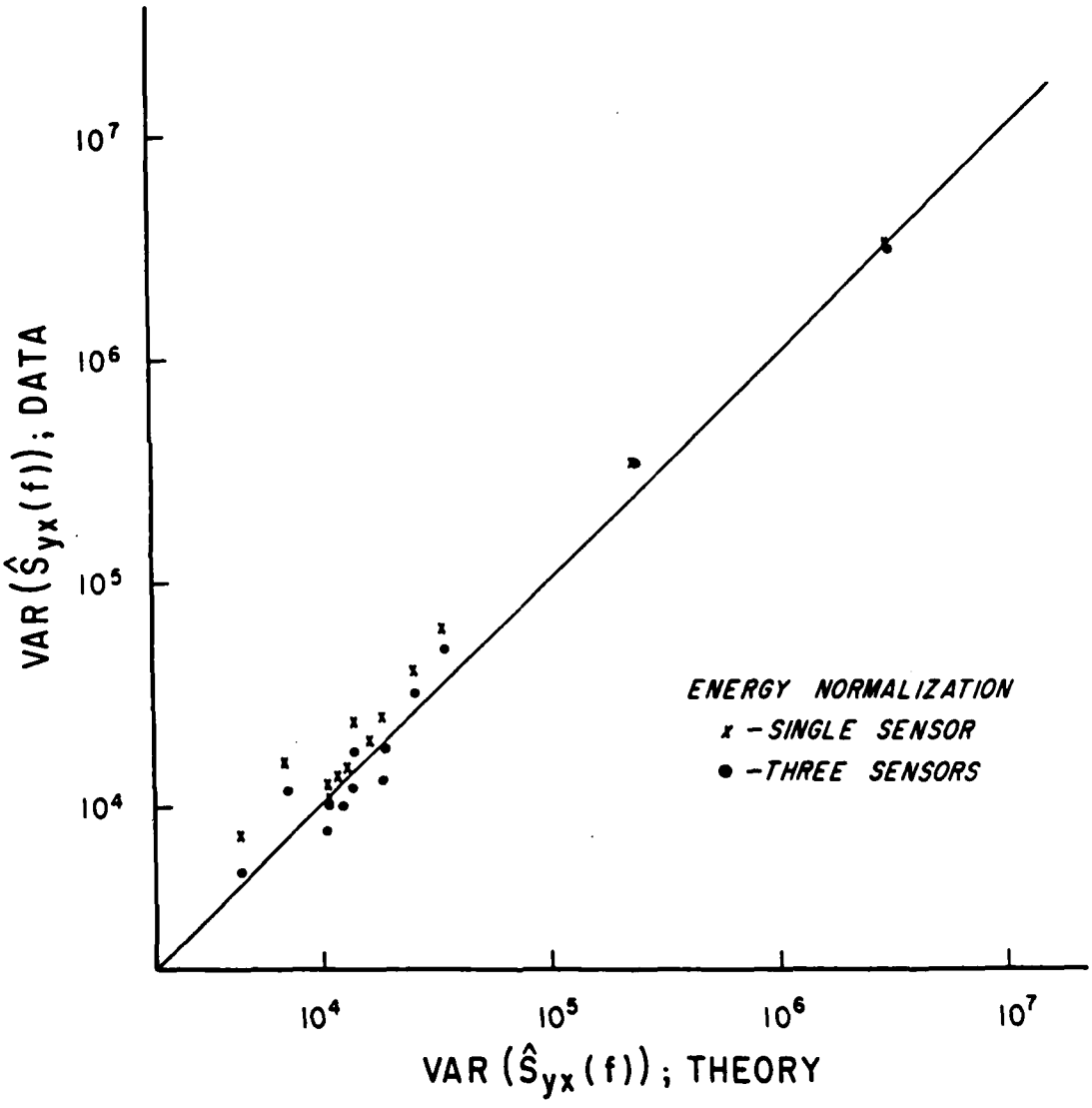


Figure A1-3. Comparison of theoretical values of the variance of $S_{yx}(f)$ estimates with sample values obtained from linear array data. The x's represent array data which is normalized to the energy density of a single sensor while the dots are normalized to an average of 3 sensors. The variances have the units $cm^4 sec^2$.

of the estimator variance. Therefore, this distribution family may be useful in the description of array estimate variability.

A 400 m length linear array, described by Pawka et al (1980), was maintained at Torrey Pines Beach, California. Sample distributions of $S_{yx}(f)$ estimates obtained from the array data are shown in Figure A1-1. These sample distributions are compared to analytic density functions which were generated using the measured directional spectra from the array. The comparisons show good agreement of the low order distribution moments. The analytic and sample variances (Figure A1-3) and skewness show very high correlation. The comparison of higher order moments were inconclusive due to the limited nature of the data sets.

Additional field data for comparisons with the theoretical distributions were sampled during the past year. Two biaxial electromegnetic current meters, separated by 90 m, were placed in a line along the 5 m depth contour at the Torrey Pines Beach site. The 400 m array, located in a mean depth of 9.6 m, was also operated for background wave information. Roughly 5 days of long data runs (duration $\sim$6 hours) were sampled. This data will be used to further test the $S_{yx}(f)$ distributions at a single location and also the covariability of $S_{yx}(f)$ estimates made at a given spatial separation.

A1.2 Island Shadowing (S. S. Pawka and D. L. Inman)

Torrey Pines Beach, Southern California, is partially sheltered from the deep ocean by the Channel Islands. Last year's progress report described field data comparisons with an island blocking and refraction model of the wave transformations from deep ocean to the coast. The islands were shown to significantly affect the coastal wave conditions. However, only limited confirmation of the blocking/refraction model in the mid frequency range (0.082-0.114 Hz) was obtained due to the poor quality of the estimates of the deep ocean directional spectrum.

Work during the past year was concentrated on the study of the characteristic features of the directional spectra at Torrey Pines Beach. Particular attention was paid to the estimation of wave energy density in the shadowed quadrants of the local directional spectrum. Three directional spectrum estimators, two of which were developed in this study, were compared for their quanitative performance in the definition of the spectral features. The results indicate consistently low energy density levels in the shadowed quadrant associated with San Clemente Island (SCI) in the mid frequency range. The spectra at higher and lower wave frequencies occasionally contain significant energy density in this shadowed quadrant.

The directional sectors $\alpha_\infty$ = 264.5-277°T (SCI) and $\alpha_\infty$>291.5°T at Torrey Pines Beach are blocked by islands and the coastline. The island blocking/refraction model predicts zero energy density in three sectors of the local deep water directional spectrum. Extensive model tests were used to show that the Maximum Likelihood Estimator (MLE), a widely used directional spectrum technique, yields biased-high estimates of the energy density in

these directional "gaps". Two alternative estimation techniques were developed. The first method attempts to deconvolve the smearing effects due to the limited array size by making iterative modifications to the MLE estimate. The resultant spectrum (IMLE estimate; Pawka, in prep.) smears through the array's windowing filter to yield the original MLE estimate. In this sense, the IMLE estimate is a possible solution for the "true" directional spectrum. The second estimator attempts to "minimize the square window" error in forming its estimate at each look angle. The derivation of this estimator (MSWE) follows the basic design of the Steered Apriori Optimal Estimator developed by Regier (1975). The directional spectrum estimate is formed from weighted sums of the measured cross-spectra. The weights are adjusted to minimize the square error due to the windowing of the measured MLE directional spectrum subject to the constraint that energy density at the look angle is passed unaltered. A noise rejection term is also added to the minimization equation. A discussion of the development of the IMLE and MSWE estimators as well as their possible applications is being prepared for publication.

A quantification of the SCI island gap definition is achieved by normalizing the energy density at the center of the gap, $E_g$, by the total frequency band energy, $E_{tp}(f)$. The various estimates of this ratio for a data set on 5 March 1977 are shown in Figure A1-4. The MLE estimates of "normalized" gap energy are biased-high relative to the other results for all wave frequencies. The IMLE and MSWE estimates agree well, particularly in the range 0.121-0.145 Hz. The IMLE estimates in the mid frequency range

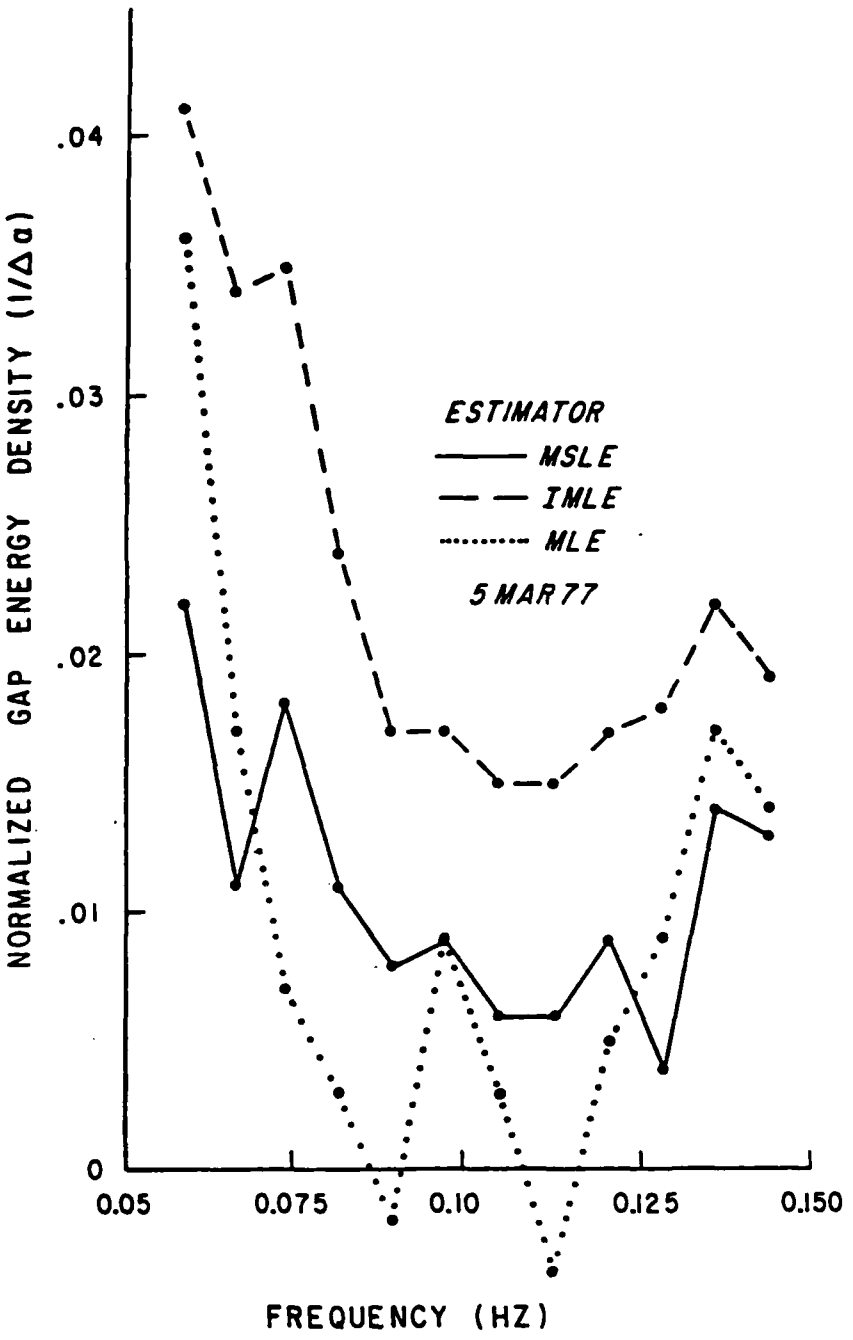


Figure A1-4. Normalized San Clemente Island gap energy density on 5 March 1977. The results are averaged over 14.3 hours of continuous data. The directional bandwidth is 1° and the frequency bandwidth is 0.0078 Hz.

are more stable than the MSWE results but show a small relative bias (high). The IMLE directional spectra show the sharpest definition of the gap in the lowest frequency bands. All of these low to mid frequency results on 5 March 1977 data match predictions made from model testing the estimator responses to model spectra with very low gap energy density.

High quality data from 10 days of the Seasat West Coast Experiment were analyzed with the MSWE method. The results in the frequency range 0.082-0.114 Hz show negligible levels of energy density in the center of the SCI gap. The average directional spectrum, refracted out into local deep water, for 0.114 Hz (Figure A1-5) has a sharp trough at ~271°T which corresponds to the SCI gap. Variations in the gap energy density level over the data runs did not correlate with any tested parameter of the wind or wave fields. This low level of mean gap energy density is consistent with the island blocking/refraction modeling of the wave transformations from deep ocean to the coast.

There is evidence of significant SCI gap energy levels in both the low and high frequency regimes for this data set. The average 0.145 Hz spectrum, also shown in Figure A1-5, has a raised gap level relative to the 0.114 Hz spectrum. The high frequency gap energy density correlates well with the local wind measured at the NUC tower, Mission Beach. The likely cause of the low frequency gap energy density was not determined. The maximum value of the gap energy density at all frequencies was 20% of the peak levels in the directional spectrum. Therefore, the total energy contained

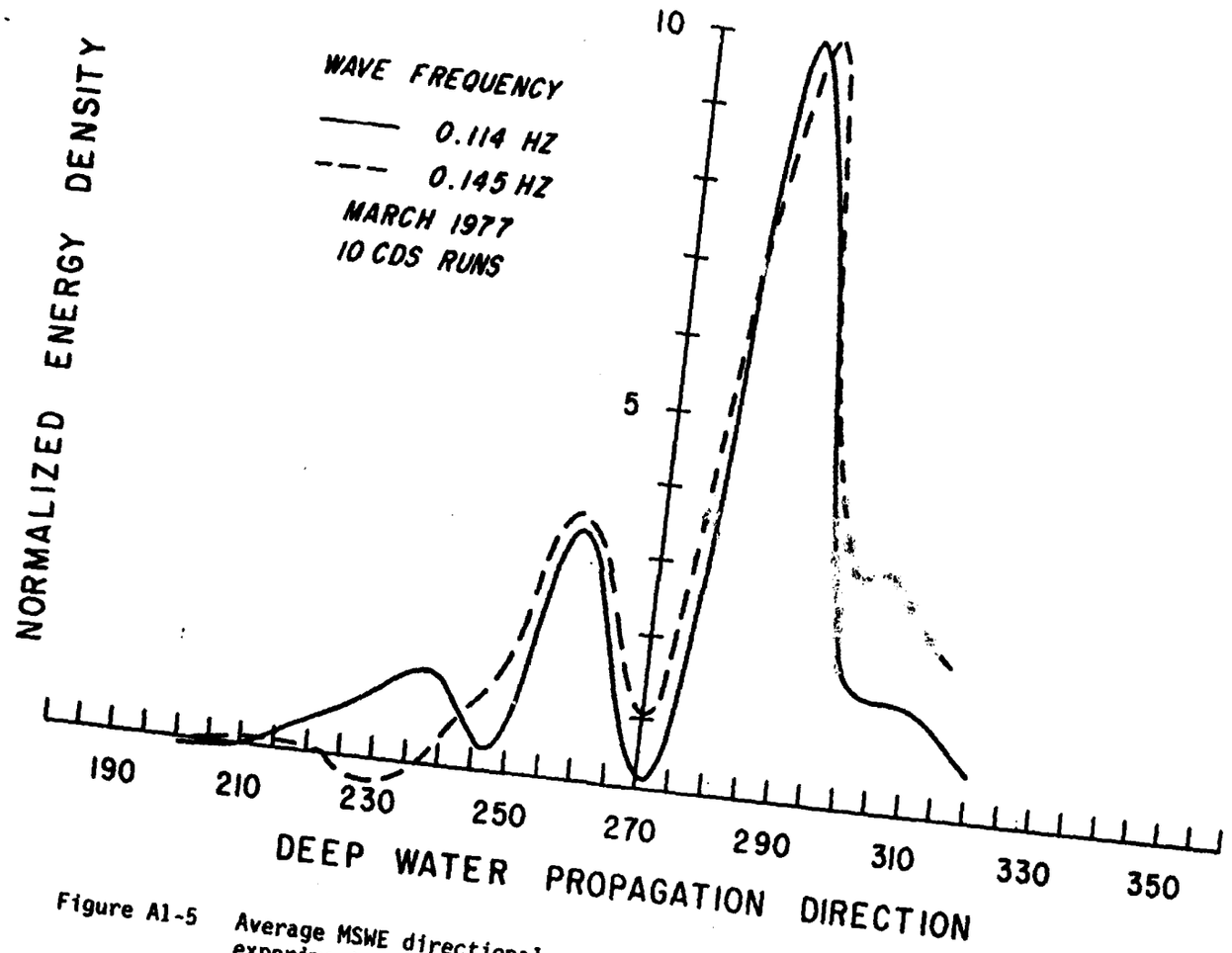


Figure A1-5 Average MSWE directional spectrum estimates for 10 days of the March 1977 experiment. The spectra have been refracted out into local deep water. The data runs have a cumulative length of about 64 hours. The spectra are each normalized to a maximum value of 10 (relative units).

in this 12.5° sector is negligible for most spectral applications.

There is a 15° directional sector at Torrey Pines Beach centered on 305°T which is totally blocked from the deep ocean but has a fetch of 250-300 km. The MSWE spectra at frequencies greater than 0.114 Hz occasionally show a directional peak associated with this "inter-island" fetch (Figure A1-4). The energy contained in this spectral peak correlates well with the local wind. The peak frequency of the energy associated with this directional sector during local wind events (wind speeds 8-10 m/sec) was 0.137 Hz. This corresponds well with the values computed from limited fetch relationships (Hasselmann et al., 1973). This peak can contain up to 30% of the total energy density in the high frequency directional spectra. This significant energy level combined with the relatively high angle of these waves with respect to the coast cause this spectral feature to be an important consideration for nearshore processes such as longshore currents. Therefore, local wind effects have to be taken into account to adequately describe the local wave field for wave frequencies greater than 0.12 Hz.

There are two persistent peaks in the directional spectra at Torrey Pines Beach associated with waves propagating to the site from the North Pacific. The peak with mode direction ~285-290°T is due to waves coming through the primary window between the Channel Islands while the southern peak ($\alpha_{\infty}$~255-260°T) is due to refraction over banks and shoals south of SCI (Pawka, in prep.). Accurate estimates of the relative energy in these two prominant peaks is a necessity for quanitative utility of the directional spectra. Ratios of the energy contained in these two peaks, obtained from

the various directional spectrum estimators for 5 March 1977, are shown in Figure A1-6. The MSWE and IMLE estimates are in close agreement for the frequency range 0.114-0.145 Hz, while the MLE estimates show a considerable bias. The MLE estimates have the most significant deviation from the results of the other methods for the high frequency range.

Data comparisons presented here and extensive model testing (Pawka, in prep.) have shown that the MLE method is quantitatively deficient for many desirable applications of the directional spectra. The results also indicate improved relative performance on the IMLE and MSWE methods. However, no single method is recommended at this time as an "optimal" estimator for general application. Intercomparison of the results of several methods has proven to be a useful analysis procedure. Additionally, alternative estimation techniques, tailored to address specific quanitative questions, may prove to be more desirable in limited application.

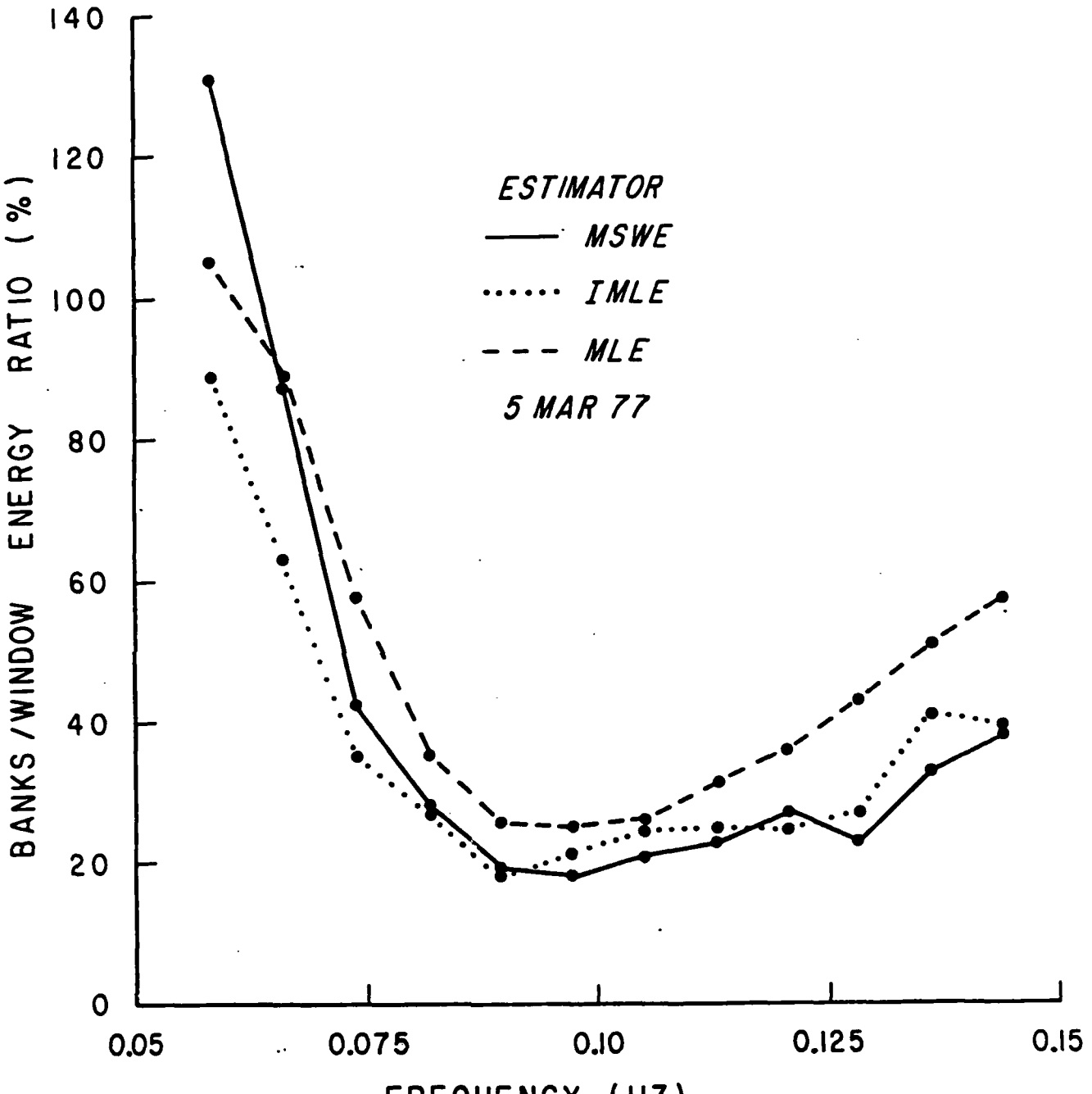


Figure A1-6. Ratio of the banks quadrant (250-269°T) to northern window (270-296°T) energy for the various directional spectrum estimators. The low frequency ratio is the highest due to the strength of the refraction process. The rise of the relative importance of the banks quadrant energy at higher frequency is due to the broadening of the deep ocean directional spectrum.

A1.3 Shoaling Waves (M. H. Freilich)

The aim of the shoaling waves task has been to develop and test a model describing the changes undergone by wind generated surface waves (4-18 sec period) as a broad spectrum of such waves propogates shoreward over a sloping bottom. A one-dimensional theoretical model based on the Boussinesq equations and incorporating the physics of multiple triad near-resonance has been derived and implemented numerically. The model, which assumes that all waves are normally incident to the beach, has no "free" or empirically determined parameters. A single field experiment can thus be used to determine the operational validity of the model and the assumptions that are incorporated in its derivations.

Such a field experiment, involving dense instrumentation of the shoaling region from 10 m depth to 3 m depth was conducted from June to September 1980. A plan view of the experiment is shown in Figure A1-7. Much of the data acquired in the experiment has been analyzed in light of the Boussinesq model, and the results are very encouraging.

As shown in Figures A1-8, 9, 10, the model appears to do an excellent job predicting the evolution of the spectrum of sea surface elevation throughout the shoaling region. The model predicts spectral shapes significantly better than does linear theory over a broad range of input conditions.

Since the Boussinesq model predicts component amplitudes and phases, not just gross spectral quantities, higher order moments such as skewness of depth averaged velocity can be computed and compared with data. Both the model and the data show a significant increase in negative skewness (corresponding to higher shoreward velocities and peaked wave crests) as the waves propogate shoreward through the shoaling region, as shown in

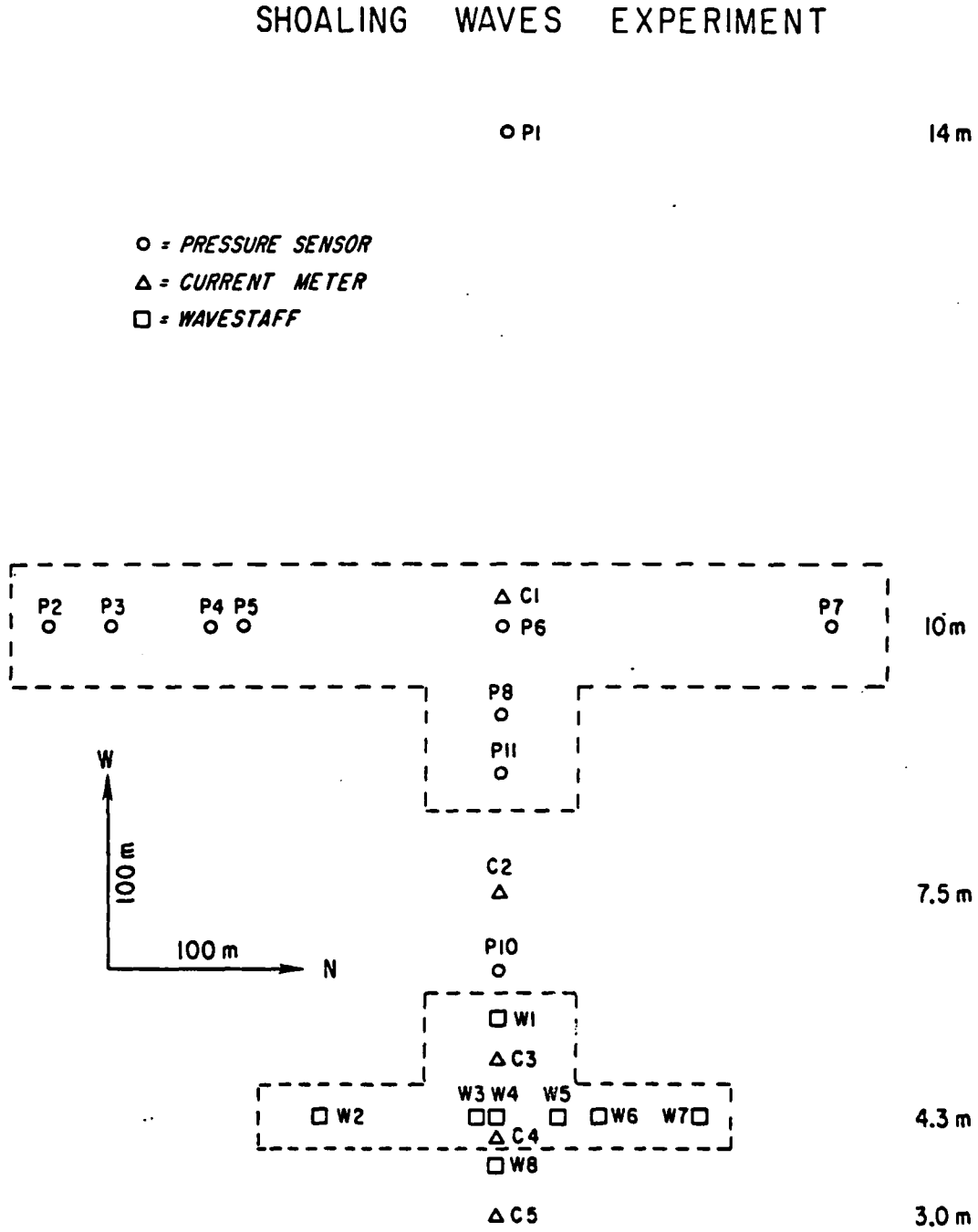


Figure A1-7. Plan view of the instrument locations in the 1980 shoaling waves field experiment. Approximate depths are given near the right side of the figure.

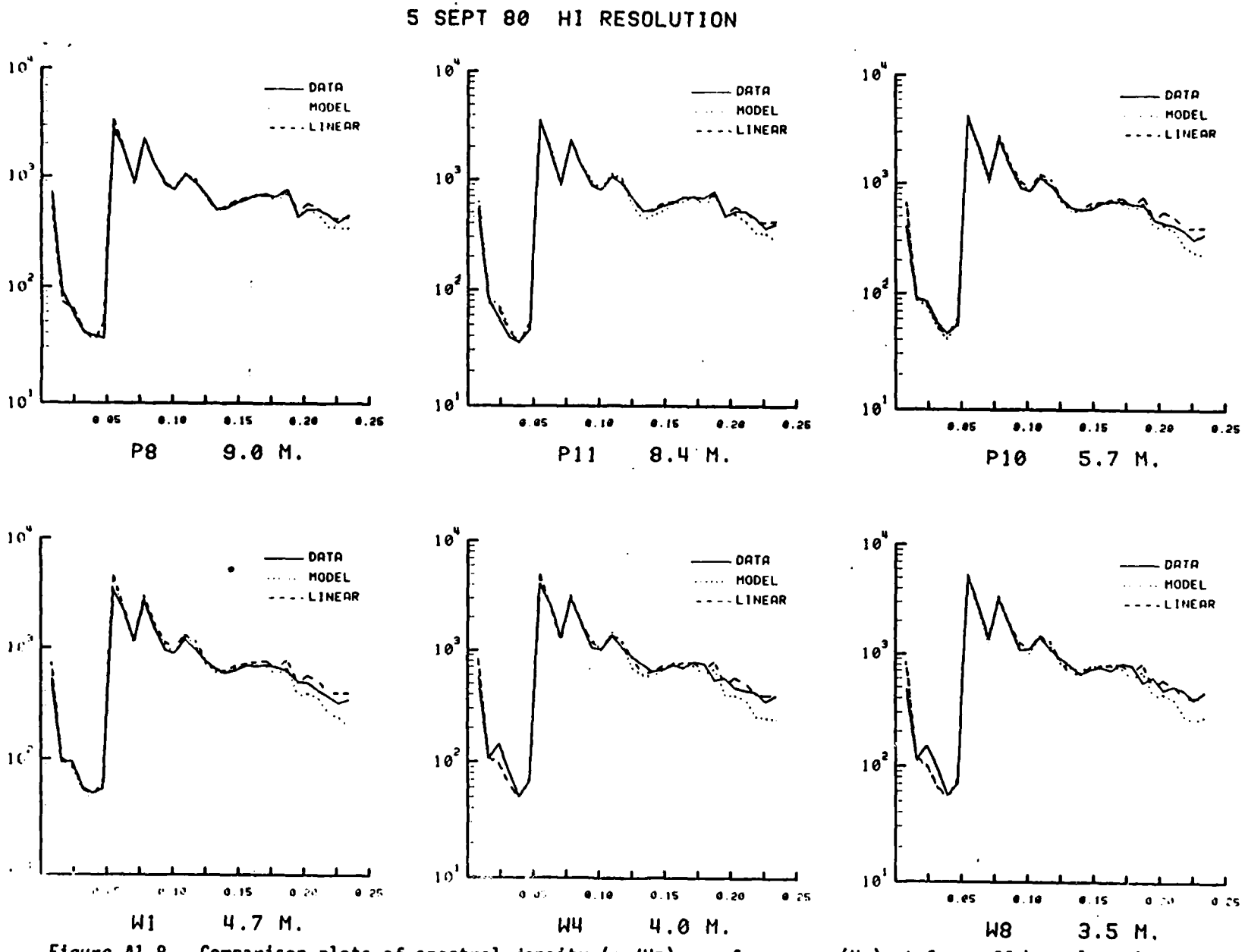


Figure A1-8. Comparison plots of spectral density (cm/Hz) vs. frequency (Hz) at 6 on-offshore locations. Each plot shows the actual data at the indicated depth, the prediction of the Boussinesq model, and the prediction of linear theory. Both the Boussinesq and linear theory predictions are based on a 240 mode decomposition of the 10 m data. This day (5 Sept 80) has very low energy and a broad spectrum. Note that both linear theory and the Boussinesq model predict the spectrum well.

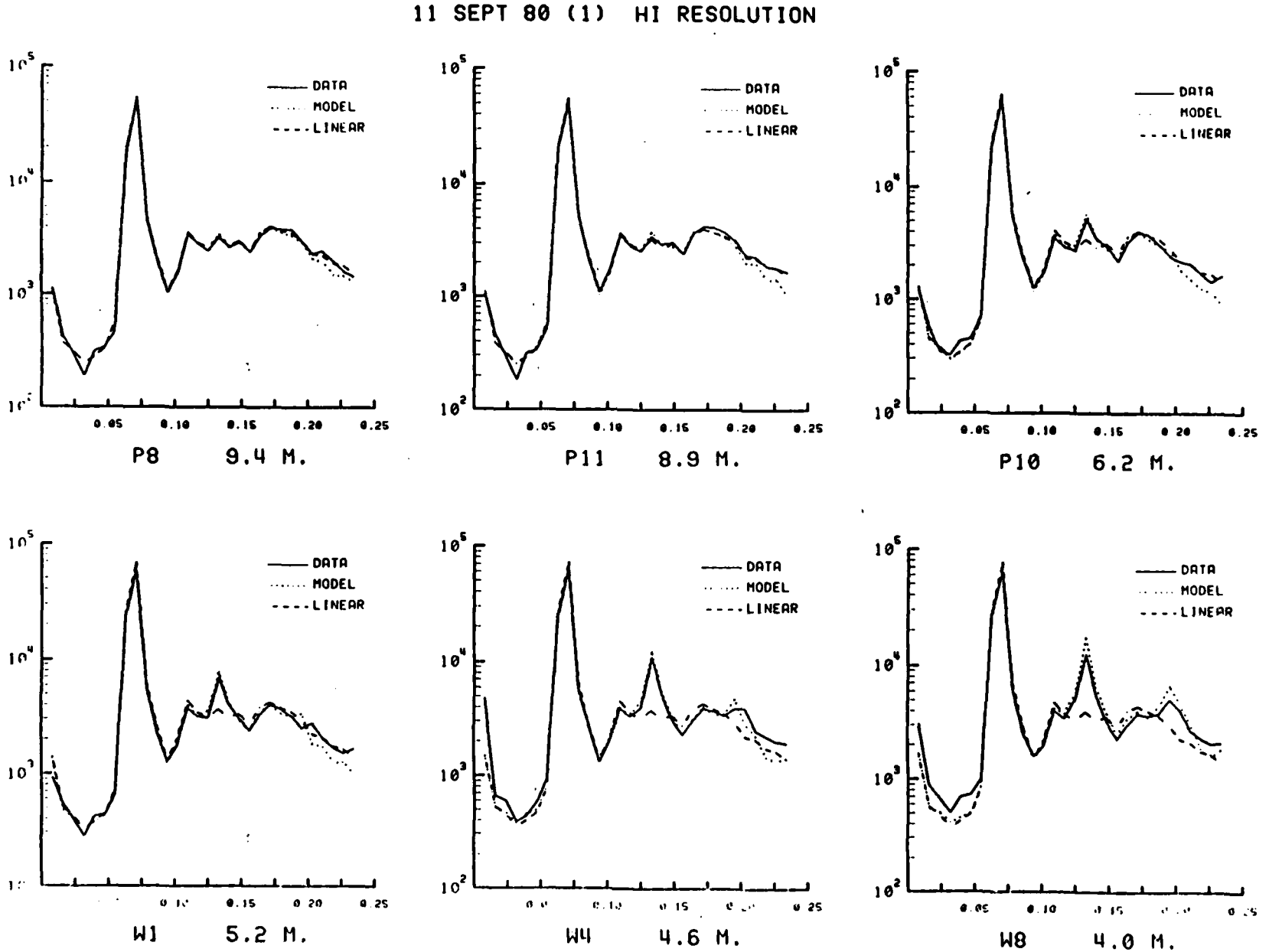


Figure A1-9. Same as Figure A1-8, but this day (11 Sept 80) is characterized by a very narrow spectrum as measured in 10 m depth. Linear theory cannot predict the increase of harmonic energy as the waves propogate shoreward.

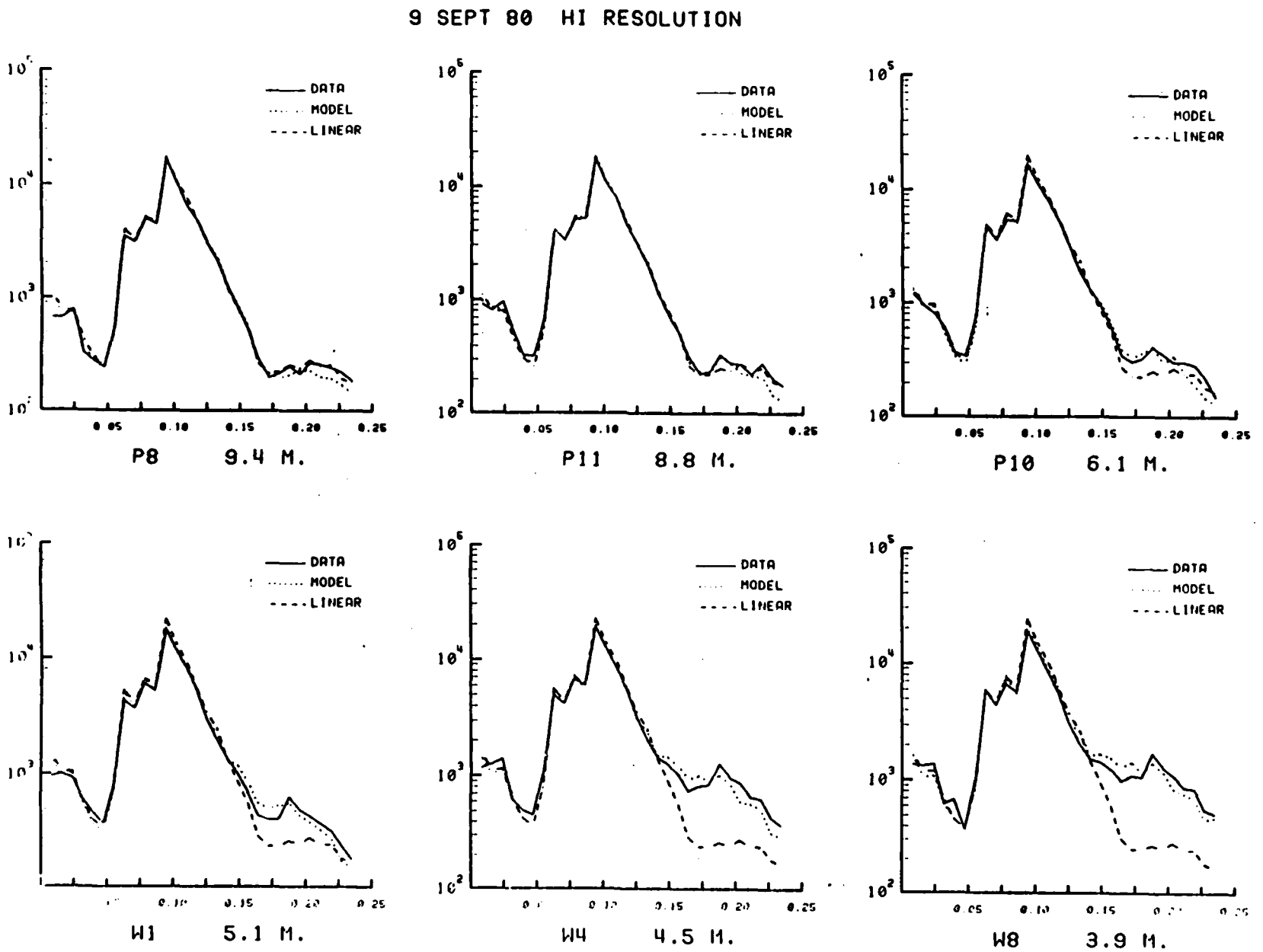


Figure A1-10. Same as Figure A1-8 for a high energy, broad spectrum (9 Sept 80). Neither linear theory nor a monochromatic Stokes-type theory could predict the general increase in a broad high frequency band observed on this day. The Boussinesq model, however, predicts the spectral shape changes well.

Figure A1-11. Although quantitative agreement between model and data is not as good as for spectral comparisons, the model predictions are always within a factor of 2 of the data.

Dissipation of wave energy through the shoaling region is expected if energy is being extracted from the waves due to bottom stress. Both the data and the Boussinesq model exhibit non-conservation of energy flux computed from linear theory through the shoaling region (Figure A1-12). As the model contains neither dissipation nor generation, the apparent decreases and increases of linear energy flux are an indication of the inappropriateness of linear ideas applied to even weakly nonlinear systems. The fact that the model predictions are quantitatively similar to data at the 3% level indicate that dissipation in the shoaling region before the break point is, in fact, small.

In a model independent analysis, the data obtained by the two wave directional arrays (enclosed by dashed lines in Figure A1-7) is being used to determine the amount and frequency distribution of seaward propogating (reflected) energy in the wind wave band. Preliminary results show that the outgoing energy is small (<10%) compared to the incoming energy over a wide range of conditions.

Theoretical model. In order to be applicable to field situations, any theoretical shoaling model must allow for a complicated wave field composed of a braod, arbitrary frequency spectrum.

Two basic types of models have been used in the past to predict the wave field parameters of surface elevation, pressure, and particle velocity in the shoaling region: Linear theory, and forced nonlinear (Stokes) theories. Linear theory is based on the assumption that nonlinear terms in

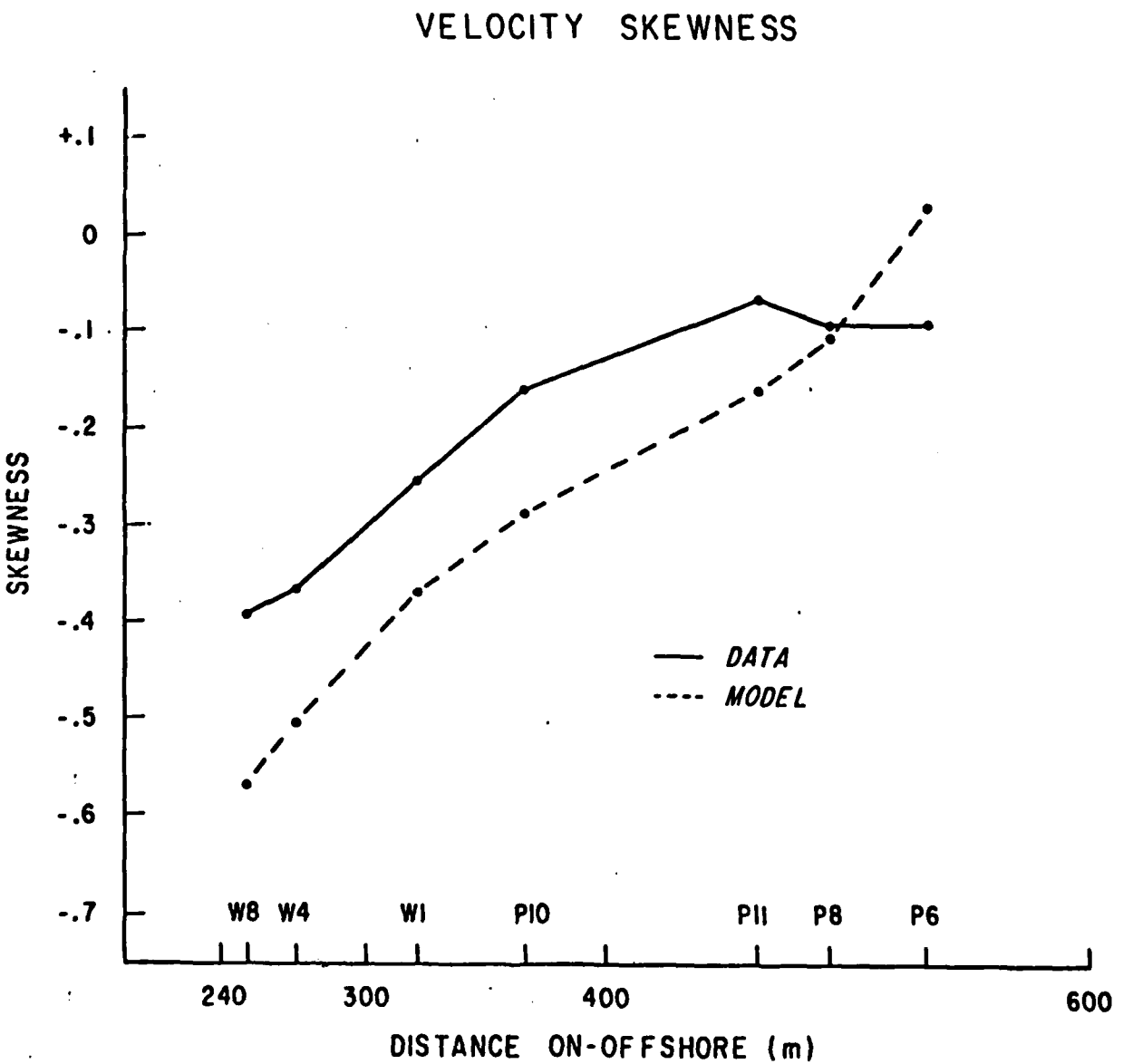


Figure A1-11. Skewness of depth-averaged velocity versus on-offshore distance from both the data (solid line) and model (dashed line). The model skewness was constrained to start with near-zero skewness at location P6.

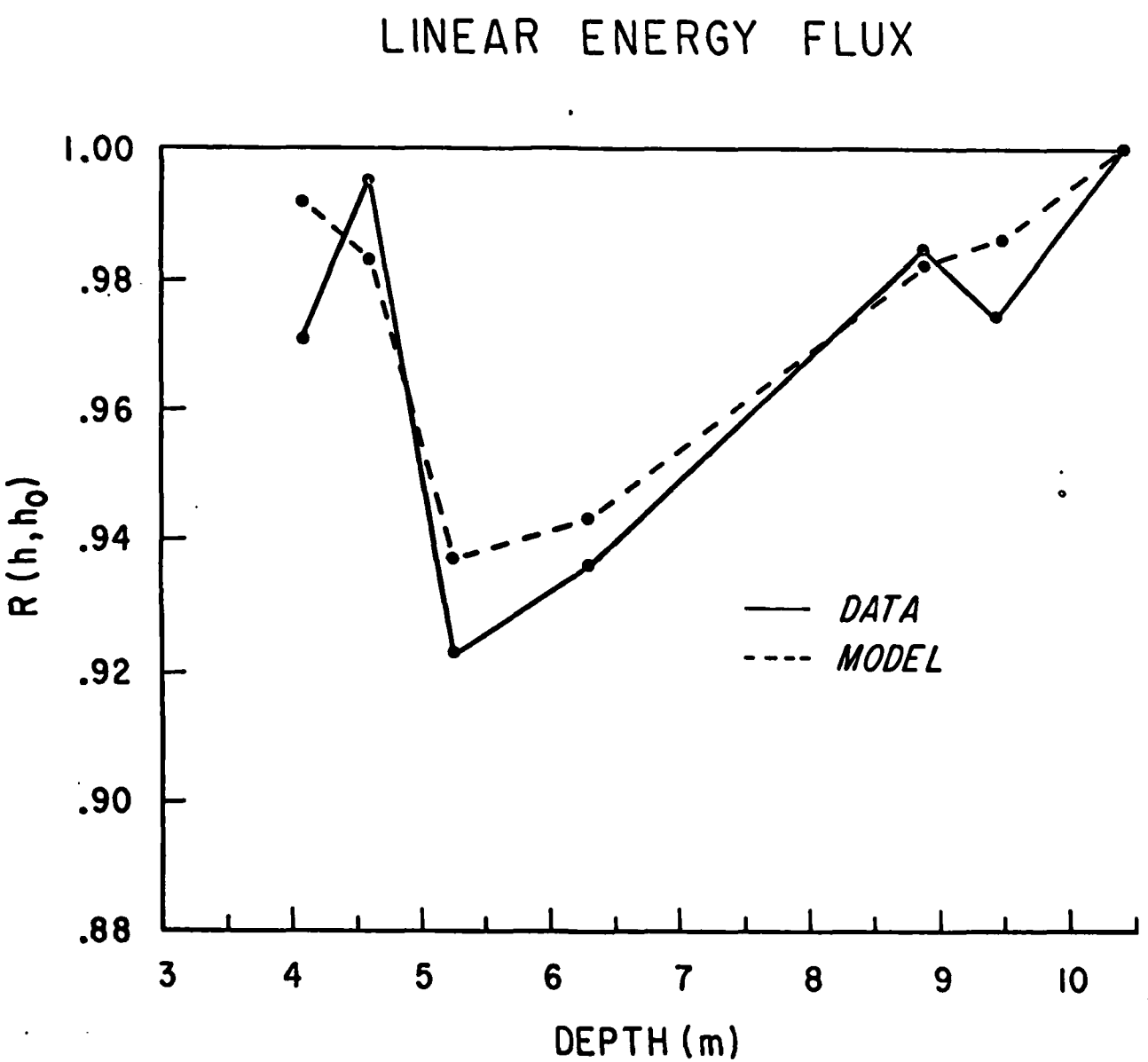


Figure A1-12. Comparison plot of $R(h,h_o)$ versus depth for 11 September 80 ($h_o$=10.3m). If linear energy flux were conserved, $R(h,h_o)$ would be a constant $R(h,h_o) = 1$. The fact that the model compares well with data indicates that $R(h,h_o)$ is not a conserved quantity for a nonlinear system such as shoaling surface gravity waves.

inviscid, irrotational equations of motion and boundary conditions are unimportant. The resulting equations can be solved analytically even for a wave field of arbitrary spectral shape. The solutions conserve energy flux and predict a general increase in sea surface elevation as the waves propogate shoreward. However, the model has many drawbacks: bottom slopes must be extremely small, and amplitudes of waves long in comparison to the depth must be unrealistically tiny for the linearization to remain consistent. Since the theory itself predicts increasing amplitude for decreasing depth, this latter condition, even if true initially, is quickly violated. In addition, linear theory predicts that wave forms remain symmetric throughout the shoaling region and cross-spectral energy transfers do not take place, both in obvious contradition to observations.

Forced nonlinear theories take into account the modifications to a single linear wave train when its amplitude becomes finite. The solution for the wave train at any given order is composed of the fundamental wave and its forced harmonics. Considerable effort has been expended in the development and testing of such theories. Well known perturbation methods can be used to derive algebraic expressions for the relative amplitudes of the fundamental and harmonics. Flick, et al (1981) have shown that such solutions valid in deep water can be matched to cnoidal wave solutions valid in shallow water. In addition, these workers under ONR sponsorship have conducted extensive laboratory testing of the solutions. Unfortunately, monochromatic forced solutions are inappropriate to cases where the offshore wave spectrum is broadbanded in frequency. Algebraic complexity grows rapidly as more fundamental waves are added and the matching to shallow water solutions is no longer valid. Even in the monochromatic case, the

model cannot predict the evolution of the assymmetric wave forms characteristic of waves near breaking.

In response to the above deficiencies of both linear theory and forced nonlinear theories, we have developed a shoaling model based on the Boussinesq equations and the physics of multiple triad near resonance across the entire wind wave frequency band. The "Boussinesq model" currently allows for waves propogating only normal to a beach with parallel contours. In addition, it is not clear how the model can be matched in an analytic way to Stokes-type descriptions of deep water waves. However, the model predicts the evolution of both broad and narrow banded input spectra, and it allows for the development of asymmetric wave forms. For a detailed derivation of the one dimensional Boussinesq shoaling model, the reader is referred to Task (80-2) of the 1980 ONR progress report.

The model is cast as a set of coupled, first order differential equations for the on-offshore evolution of amplitudes and phases of the Fourier modes of the wave field. The model contains no adjustable parameters or empirically determined constants. It can thus be directly tested against data. The plan view of an experiment designed to test the model is shown in Figure A1-7. The experiment design was discussed extensively in Task (81-2) of the 1981 ONR proposal. Comparison between data from the on-offshore instrument transect and predictions of the Boussinesq model is straight forward. Each of the 17.1 minute records of data at each on-offshore location are reduced and transformed to yield Fourier components of depth averaged velocity. A spectrum composed of 240 modes from location P6 (approximately 10 m depth) is used as the initial condition for the numerical integration of the model's coupled evolution equations.

Spectral Evolution. Spectral comparisons between the model predictions and data can be made at each on-offshore location. Figure A1-8 shows such comparisons at 6 locations, ranging in depth from 9.0-3.5 m on 5 Sept 80. The dashed third line on each plot represents linear theory predictions of spectral density. This particular data is an example of a broad banded, very low energy wave field ($\bar{H}_s$ in 9.9 m depth is 38 cm). As expected with such small waves, nonlinear effects are small, and both linear theory and the Boussinesq model predict spectral shape well.

Figure A1-9 is a similar comparison on 11 Sept 80. The offshore spectrum is quite narrow, with most wave energy concentrated in a peak centered at 0.065 Hz. ($\bar{H}_s$ is 90 cm). Spectral evolution is seen to be characterized by the emergence of a major narrow peak centered at 0.127 Hz, and a smaller peak at 0.190 Hz. Although linear theory does not predict these peaks at all, the Boussinesq model accurately predicts both their locations and amplitudes throughout the shoaling region.

Figure A1-10 presents yet a third comparison, using data obtained on 9 Sept 80. In this case, the spectrum in 10.3 m depth is fairly broad, and the waves are of moderate height ($\bar{H}_s$ is 66 cm). A dramatic evolution of the spectrum is observed, with the entire high frequency region increasing in energy. Once again, linear theory does not properly predict the spectral evolution, while the Boussinesq model compares very well with the data. The Boussinesq model is thus seen to predict spectral evolution well over a wide variety of wave conditions and spectral shapes.

Skewness. Third and higher moments of the wave field have been shown to be important to sediment transport processes (Task B2). In water deeper than 10 m, the wave field is to a good approximation Gaussian, and

thus all odd moments are exceedingly small. Previous laboratory and scattered field measurements indicated that skewness of surface elevation or depth averaged velocity increases in a negative way (corresponding to sharp wave crests and large maximum onshore fluid velocities). To our knowledge, this evolution has never been measured in a detailed way in the field. The Fourier coefficients of the data at each on-offshore location can be used to calculate velocity, and the results for 9 Sept 80 are presented in figure A1-11. Also shown is the skewness as calculated from the Boussinesq model. Although the model skewnesses are everywhere larger (in a negative sense) than those calculated from data, the model predictions are well within a factor of 2 of the data. This appears to be a general result for all data analyzed so far.

Dissipation. The amount of energy lost from the wave field is of crucial importance to studies of sediment transport outside the break point. Since wave breaking and associated turbulent dissipation is not a major factor in the shoaling region (in comparison to the surf zone), detailed measurements of the "dissipation" of wave energy in this region could provide a realistic upper bound for the energy available to move sediments. The Boussinesq shoaling model alone provides no information on dissipation, as it was assumed at the outset that all viscous terms in the full Navier-Stokes equations could be neglected.

The model can be used however, to show that energy flux as calculated by linear theory is not conserved over distances comparable to the on-offshore extent of the shoaling region. The mathematics is lengthy and the formal ordering arguments needed in even the simplest cases are subtle, and will not be reproduced here. We present instead comparisons between

total linear energy flux as calculated from the data at various on-offshore locations, and the same quantity as calculated from model integrations. At any depth or on-offshore location, the total linear energy flux density can be defined as:

$$F(h) = \int [a(\sigma)]^2 \frac{\partial \sigma}{\partial k} \, d\sigma$$

where $[a(\sigma)]^2$ is the spectral density of surface elevation at frequency $\sigma$, and $\frac{\partial \sigma}{\partial k}$ is "group velocity" calculated from the linear dispersion relation. In a dissipationless linear system, $F$ is constant, independent of $h$ or on-offshore distance. A measure of non-conservation of $F$ is given by:

$$R(h,h_o) = F(h)/F(h_o)$$

The effect of dissipation on the linear system would be to cause $R(h,h_o)$ to decrease monotonically for $h<h_o$ for waves propogating towards the shore. An observed increase in $R(h,h_o)$ could be due to a localized source of wave energy, which is unlikely.

The solid line in Figure A1-12 presents a typical example of the behavior of $R(h,h_o)$ as calculated from the data. In this case, $h_o$ is 10.3 m. Note that $R(h,h_o)$ both increases and decreases appreciably through the shoaling region. The dashed line presents an identical calculation made using the results of a model integration. Here also $R(h,h_o)$ clearly is neither constant nor is its behavior monotonic. It should be remembered that the model lacks any mechanism for either dissipation or generation. Thus, the nonconservation of $F(h)$ in this case is a strong indication that $F(h)$ is not a conserved quantity for a weakly nonlinear, multiply resonant system such as shoaling waves. The fact that model predictions of linear

energy flux are quantitatively similar (±3%) to local calculations from the data, can be used to construct the argument that total dissipation from the wind wave frequency band must be small through this shoaling region. It is clear, because of nonlinear effects, that experiments which measure only wave field parameters have limited utility as direct tests of the importance of dissipation.

Outgoing Energy. Data from the two directional arrays (enclosed by dashed lines in Figure A1-7 ) can be used to construct full, 360° directional spectra in the wind wave frequency band. It is hoped that this data will eliminate the need for doing a completely new experiment to test a future two-dimensional shoaling model. In a purely descriptive sense, the data from the arrays can be used to characterize outgoing (seaward propogating) energy in the shoaling region.

Such energy could be caused either by gradual reflection from the sloping bottom, or the highly nonlinear processes dominating the surf zone. Preliminary results from the current experiment indicate that outgoing energy is small ( 10% of incoming energy) in the wind wave band. The Maximum Likelihood Estimator used to process array data cuases energy to spuriously appear to be seaward propogating. Thus extensive model testing is necessary to quantitatively discuss outgoing energy. However, these preliminary results confirm the utility of linear longshore arrays for measurements of nearshore wave directions.

A2. Shelf Waves (R. T. Guza)

Shelf waves are defined here as oscillations confined to coastal regions because of topographic trapping effects associated with shelf and beach bathymetry. Shelf waves considered in this task have periods ranging from 1 to 10's of minutes, and horizontal length scales from 100's of meters to 10's of kilometers. Various kinds of shelf waves are thought to be important elements in harbor seiching, currents on the continental shelf and surf beat. The long term goal of this task is to assess the relative importance of shelf waves in various physical environments and to identify the mechanisms leading to their excitation. Effort so far have been concentrated on surf beat, since this is a phenomenon of first order importance to the inner surf zone velocity field.

Surf beat are the low frequency (periods of one to several minutes) oscillations which typically contain a substantial portion of the energy observed in inner surf zone elevation and velocity fields. Surf beat has its maximum energy levels in the run-up. During the past contract year, a large amount of run-up data consisting of time histories of the swash/dry beach intersection point previously collected at Torrey Pines Beach has been analyzed. The goal of the analysis is to empirically relate the level of surf beat activity in the surf zone to the amount of incident wind-generated wave energy measured with an offshore sensor.

An important conclusion is that the magnitude of typical swash excursions, $\tilde{R}_s^H$ increases approximately linearly with increasing incident wave height $\tilde{H}_s$. Figure A2-1 shows the linear trend (solid line) for a variety of incident wave conditions. When the swash excursions across the

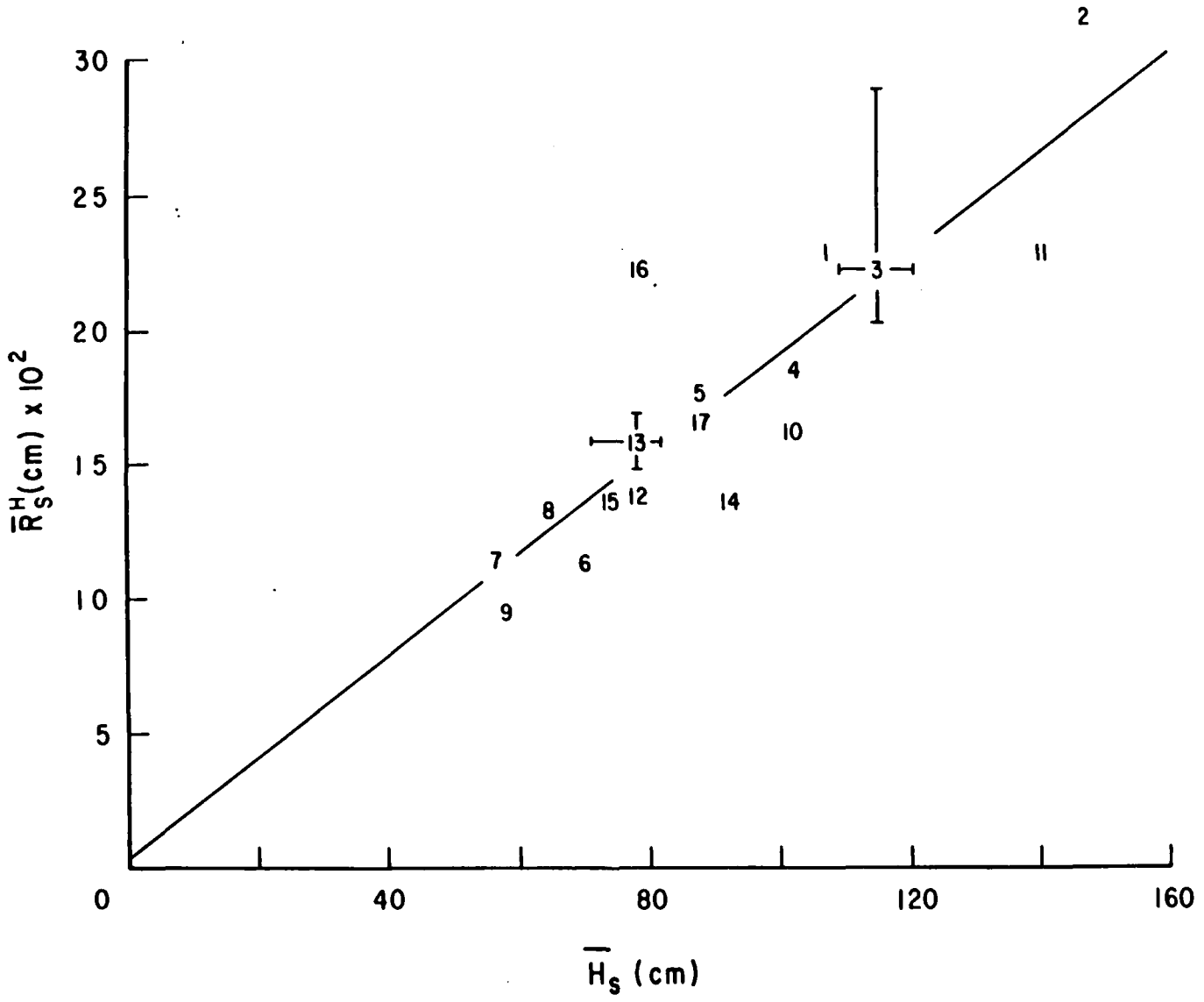


Figure A2-1. Averaged significant wave height in 10 m depth $\bar{H}_s$ versus run-up excursion $\bar{R}_s^H$. Brackets show typical range of values for the individual data used in each average. Each symbol (number) represents a data run of several hours.

beach face are transformed to vertical displacements, significant vertical run-up heights are found to be roughly 70% of the significant height of the incident wind waves at 10 meter depth.

Previous ONR supported work (for example Inman et al., 1968) pointed out that typical run-up spectra show low frequency (surf beat) oscillations to be more energetic than run-up motions at wind wave frequencies. The present data set was used to quantify that observation by dividing the run-up energy into low and high frequency components. A frequency of 0.05 Hz (period 20 s) was chosen as the highest frequency considered to be part of the surf beat motions. Figure A2-2 shows that the high frequency portion of the run-up (numbers in circles) remain approximately constant with increasing $\bar{H}_s$, while the surf beat varies linearly. On the day with the largest incident waves, surf beat swash amplitudes are about six times that of the wind wave frequencies. In the inner surf zone, the presence of large amplitude surf beat motions is probably the most important dynamic consequence of energetic incident waves and a wide surf zone. Details of the above work are given in Guza and Thornton (in press).

The motions at surf beat periods are probably related to variations in the heights of incident waves. There is also a surf zone response to the mean incident wave height. The mean water line at the shoreline is elevated ("set-up") above its location in the absence of waves. The Torrey Pines run-up data (Figure A2-3) shows that the shoreline set-up $\bar{\eta}_M$ is about 17% of the deep water significant wind wave height, $\bar{H}_{s\infty}$ (Guza and Thornton, 1981).

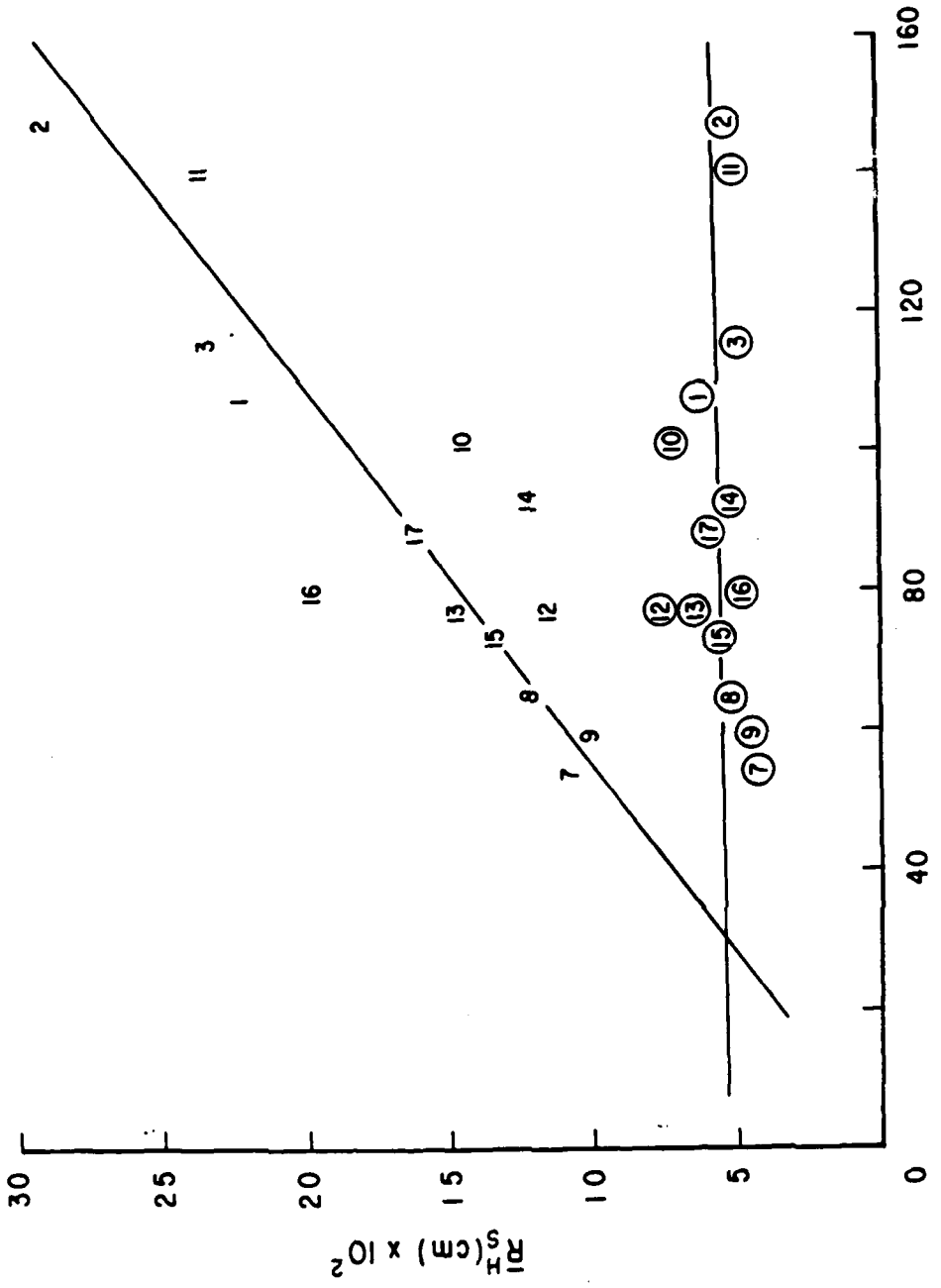


Figure A2-2. $\bar{H}_s$ versus low and high frequency components of run-up excursion $\bar{R}^H_s$. Each number represents a data run of several hours. Encircled numbers are high frequency components.

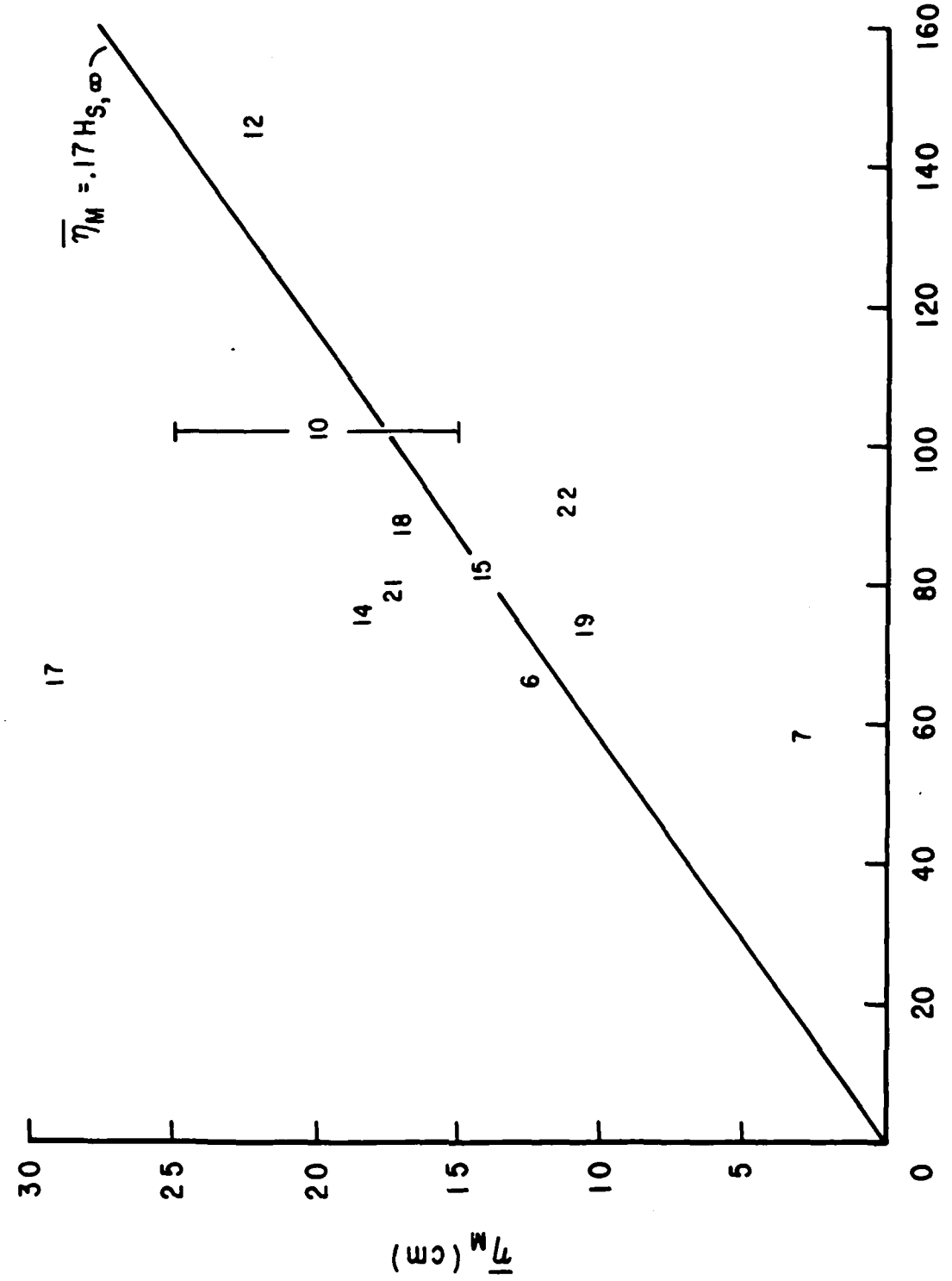


Figure A2-3. Shoreline set-up versus significant height of incident waves.

## A3. Surf Zone Dynamics

### 3.1 Turbulence (R. E. Flick and R. T. Guza)

Dividing surf zone fluid dynamics in a frequency/wavelength sense, a substantial amount is known about motions in the fluid interior in the typical wind wave frequency band, less about surf beat, still less about the high frequency gravity wave range and, essentially nothing about turbulent fluctuations. In spatial terms, the least understood areas are very near the water surface and bottom. Unfortunately, the single most important fluid dynamical topic for sediment transport is probably the turbulent bottom boundary layer, as detailed in Section B1.

Work on this task has begun during the past contract year and it is closely related to the bedload investigation of oscillatory bursting discussed in Section B1.1. This task proposed a field study of the gross characteristics of naturally occurring, rough turbulent flow in and near the surf zone under sheet flow conditions.

Progress has been made in the design and fabrication of temperature and velocity sensing instruments and mounting platforms for their deployment. A rigid platform has evolved based on the very strong and extensively tested "surf spider". This triangle based, slender legged apparatus was developed to hold current meters, wave staffs and other instruments in the swash and shallow surf zone. The legs were modified to hold the spider rigid underwater in such a way to result in minimum disturbance to the flow.

A cone probe hot film anemometer sensor has been purchased and packaged for deployment. Laboratory calibrations for speed and directional

sensitivity are underway. The low-frequency portion of the anemometer signal will be compared to an electromagnetic current meter during actual data runs to assess calibration reliability of the cone probe.

Fast response thermistor probes and circuitry have also been assembled and are awaiting calibration. This system will be used to detect small scale temperature fluctuations which may affect the hot-film anemometer measurements.

A4. Current Measurements by Geomagnetic Induction (R. E. Flick)

Progress during the contract year has been made in the design and construction of stable silver-silver chloride electrodes and of a salt bridge water-chopped system. Both these will be deployed in early fall 1981 across Mission Bay Channel. The goal of this deployment, detailed in last year's proposal, is to measure the tidal transport induced electric potential across the channel. Corrections for bottom conductivity will then be applied and the resulting estimates of volume transport compared with predictions from various theories which seek to model the flow forcing. To the extent that long waves on the shelf force bay mode resonances, this task is connected to exploratory measurements underway and proposed under Task A2.

The electrodes are much larger than those previously used in the unsuccessful attempts to measure cross-shore electric potentials (Flick and Parker, 1980). They are also more stable and less sensitive to pressure fluctuations. These "quarter-pounder" electrodes have been developed with the advice and cooperation of Dr. Jean Filloux of Scripps.

The salt bridge water-chopped instrumentation has been designed to act like a double pole-double throw switch which alternately connects each of the two electrodes to the opposite side of the flow. This must be done to avoid polarization and compensate for drift of the electrodes over the planned one to two month measurement time.

## B. FLUID-SEDIMENT INTERACTIONS "BED RESPONSE"

The ultimate objective of this contract is the prediction of shelf and beach forms given the driving forces, the general shelf bathymetry and the nature of the bottom sediments. Accordingly, the tasks under A are directed towards defining the relevant physical properties of the driving forces; while the tasks under B, the bed response to fluid-sediment interactions, lead to an understanding of the shelf and beach forms that are the central theme of this contract. The tasks under C are largely exploratory in nature, with the general objective of determining the extent to which signatures from remote sensors can be used to define the broader spacial characteristics of driving forces, the larger scale ocean surface patterns that are characteristic of coastal zone dynamics, and the large scale, longer term changes that occur in shoreline configuration.

All bed forms result from fluid-sediment interactions that genetically divide into two primary bed form classes, "forced forms", and "interactive forms"; or, a combination of these two (Task B3.1).

Since the generality of this bed form classification appears to be valid, it forms a valuable working hypothesis for the study of fluid-sediment interactions. However, we know little about the mechanics of the interactions, nor the nature and strength of the feedback mechanisms. Since the bed responds to the fluid forces by changing its form and the bed form in turn feeds momentum and vorticity back into the fluid, interactive phenomena evolve that are far more complex than the relatively simple problem of a fluid stress over

a rough but immovable bed. In fact, the granular bed itself responds to stress by expanding its volume (dilitation) so that the nature of the granular motions within the bed become functions of both the external fluid stress and the volume concentration of the solid particles in the bed. Although this property of granular-fluid media is fundamental to bed load transport and to bed forms, its mechanics remain virtually unknown (Bagnold, 1954; Inman, 1963; Bailard and Inman, in prep; Savage, 1979).

As a consequence, three tasks, B1.1 through B1.3, under this section are studies of sand bed response to fluid stress. Task B1.1 is a study of bed response to near-breaking waves and an investigation of the possibility that this intense shear involves "oscillatory" bursting. Task B1.2 is a study of the rheology of granular-fluid material, a necessary prerequisite to understanding the quantitative aspects of sediment transport. Task B1.3 is to deploy a bedload meter to measure the thickness and velocity of the bedload under waves and currents in the field. Once the bedload due to waves and currents is known at least empirically, then a rational approach to on-offshore transport and the prediction of beach slopes can be employed (Task B2).

Task B3 is a fundamental study of the formation of shelf and beach features which will supplement the study of "Bed forms produced by fluid-granular interaction" begun as ONR Task (76-4). This general task includes the fundamental study "Bedforms produced by fluid-granular interaction" (B3.1), and a definitive study of the limiting amplitude of beach cusps (B3.2). Task B4 will provide information on coastal forms and the budget of sediment in tideless seas and may be expanded to study the mechanism of wave attenuation in shallow water.

B1.1 "Oscillatory Bursting" (D. L. Inman and S. A. Jenkins)

Bursting is a high Reynolds number mechanism in both steady and unsteady shear flow for advecting vorticity from the bottom boundary layer into the interior of the fluid. Vorticity leads to turbulent vertical velocities which in turn suspends sediments. The burst cycle starts with an instability in the boundary layer which subsequently degenerates under certain conditions. The instability could result from an inflection in the velocity profile near the boundary due to adverse pressure gradients from certain types of bed forms, or from a flexible or permeable boundary, or even from external pressures such as gravity waves. Vorticity is concentrated in the lee of the instability, and accumulates as small "turbulent spots" (e.g. Schlichting, 1979, Ch 17). Inertial shear waves known as "Tollmien-Schlichting (T-S) waves form in the shear flow in the upper portion of the boundary layer over the curvature formed by the turbulence spots. These T-S waves grow and steepen when viscous stresses are no longer sufficient to damp them out. This instability occurs when the wave length of the T-S waves become smaller than approximately $6\delta$ where $\delta$ is the boundary layer thickness. Upon becoming unstable the T-S wave breaks or bursts into the interior of the fluid.

Oscillatory Bursting: An Hypothesis. It has been thought that bursting does not occur under oscillatory waves. Jackson (1976, p. 537) states: "The writer knows of no measurements of the burst cycle in the thin boundary layers beneath wind-generated shoaling waves. The swiftly reversing flow virtually precludes rational measurement" ... and the formation of burst cycles. Also, inspection of the characteristics favoring bursting, suggest that under oscillatory motion there is much less likelihood of favorable characteristics, except under very special circumstances (Hinze, 1975).

On the other hand, there are a number of observations that suggest that a form of bursting does occur under shoaling waves. For example, Inman (1957, p. 23) observed that the higher velocities associated with waves in shallow water "appear to place the material in a state of 'sub-suspension' with the passage of each wave crest. In this case the bottom material is moved on and off shore as a thin but dense layer of suspended particles, and the discrete cloud of suspended particles which form at the crest of the trochoidal shaped ripples appears to be absent. The thickness of the layer of 'sub-suspension' although somewhat variable, is usually of the order of a few centimeters, and appears to depend on the size of the sand and on the orbital velocity and periodicity of the waves."

In general if one observes sand motion through a face plate during the passage of swell waves near the surf zone, the following sequence will occur. Assume the waves are of 10 to 15 second period, 1 meter height, over a fine sand bottom and travel in water 2 to 3 meters deep (Figure B1-1). As the wave crest approaches, the onshore velocity will

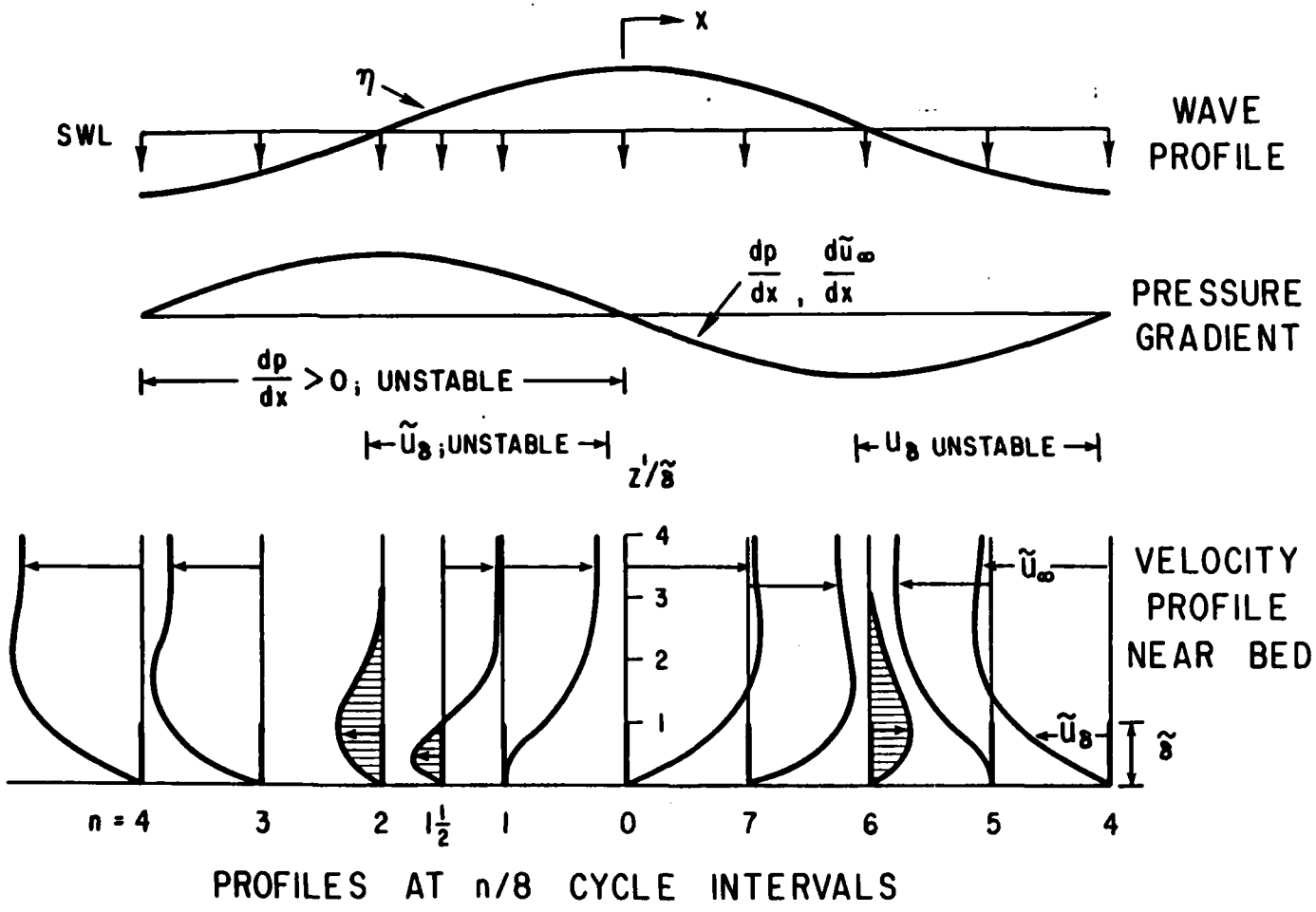


Figure B1-1. Schematic phase diagram depicting development of unstable oscillatory boundary layer under a progressive wave in shallow water. Note that both pressure gradient (dp/dx) and boundary layer velocity ($\tilde{u}_\delta$) are unstable following crest passage. Also, the thickness of the unstable portion of boundary layer increases from phase cycle 0 through 2.

rapidly increase to a threshold value and sand grains will begin to move as bedload. Then suddenly, just as the crest passes, the sand appears to "boil" and a dense cloud of sand approximately 3 to 5 cm thick moves onshore until the near bed motion is outrun by the faster traveling wave crest. The sand cloud then drops back to the bed and the bed is observed to be nearly flat, with just a faint trace of residual ripples. The ripples have wavelengths of about 6-7 cm and heights of 1/2 cm or less (e.g. Dingler and Inman 1976, fig. 9). Upon closer examination it will be noted that the sand "boils" when they occur, have an on-offshore separation approximately equal to the residual ripple wavelength, and their densest portions have more along-crest coherence as though they were associated with the remnant ripple crests.

The above phenomena is thought by us to represent "oscillatory bursting" associated with "vortex spots" in the oscillatory boundary. It is thought that the T-S waves burst because, unlike the potential oscillation in the water above, the vertically dependent phase shift of the boundary layer oscillation allows it to decelerate at the time the pressure gradient turns negative just as the wave crest passes (Figure B1-1). Oscillatory bursting is limited to a few centimeters from the bottom because only a limited region of the boundary layer supports decelerating flow under negative pressure gradients imposed by the wave profile, and exists only for a fraction of a wave cycle. Therefore the penetration distance of oscillatory bursting is limited by the onset of flow reversal.

The laminar boundary layer under oscillatory waves is given by

$$\tilde{\delta} = \left[\frac{2\nu}{\sigma}\right]^{1/2}$$

and would be about 2 mm and 3 mm thick for waves of 10 and 15 second period respectively. However, Sleath (1970) shows that the boundary layer over a flat sand bottom is rough and can be represented approximately as

$$\tilde{\delta}_r = c\ \tilde{\delta}$$

where $c$ is a dimensionless number that is a function of the Reynolds number for the sand grains and wave boundary layer, $Re = (u_m D/\nu)(D/\tilde{\delta})$. Over sand beds $c$ is of order 10, and thus the actual boundary layer thickness is about 2 cm and 3 cm respectively for 10 and 15 second waves. This boundary layer thickness is in approximate agreement with the observed 3-5 cm height of the sand "boils" associated with shallow water waves.

Experimental Investigation. The above hypothesis for "oscillatory bursting" is now being tested by field observations just outside the surf zone, using relatively simple sensors, and a short run with a hot film anemometer (a relatively complex, fragile sensor). The hot film anemometer will be used in cooperation with Task A3.1.

The study uses a motion picture camera, a pressure sensor feeding synchronous timing lights, and a high resolution sonar scanner (Dingler and Inman, 1976). If sand "boiling" is found to coincide with nearcrest passage and to have the proper length scales as postulated, then hot film anemometers will be used to sense the presence of T-S waves.

B1.2 Rheology of Granular-Fluid Material (D. M. Hanes and D. L. Inman)

One of the least understood parameters influencing bedload sediment transport is the magnitude of the bedload itself! This is a manifestation of the general lack of understanding of the physics involved in the deformation and flow of granular and granular-fluid media.

In 1954, R. A. Bagnold pioneered the field of granular-fluid mechanics by studying the flow of neutrally bouyant wax spheres immersed in fluid (Bagnold, 1954). However, because of the geometry of Bagnold's experiments, and because the particles were neutrally buoyant, there are still many unanswered questions relating to granular shear flows of geophysical interest. We think some of these questions can be answered by conducting a series of basic laboratory experiments designed to study horizontal shear flows of negatively buoyant particles.

Accordingly, an annular shear cell has been constructed in order to study the relationship between the depth of motion in a granular bed and the traction applied at the surface of the bed. Data have been collected for dry granular shear flows of spherical glass beads under a wide range of conditions.

If sufficiently intense traction is applied at the surface of a granular bed, the uppermost grains dilate and shear relative to each other. The depth to which motion occurs in the bed is believed to be governed by a dynamic yield criterion similiar to the well established Coulomb criterion for static yield. For steady shear flows of cohesionless gra ules the dynamic yield criterion relates T, the applied shear

stress, to P, the normal stress at the yield plane, by the relation $\tau = P \tan\phi_r$, where $\tan\phi_r$ is the dynamic coefficient of internal friction, and $\phi_r$ is the dynamic angle of internal friction. When applied to the case of steady sediment transport the dynamic yield criterion becomes a relationship between the bedload and the applied shear.

Since commercially available viscometric apparatus is totally inadequate for studying granular materials, a new shear cell had to be designed and built (See Figure B1-2). Shearing of the material takes place between two parallel, circular, horizontal plates. The upper plate remains stationary while the lower plate rotates. The annular gap within which shearing takes place is 4.4 cm wide with a mean radius of 12.4 cm. The shear cell was designed to permit independent control of the shear rate and normal stress. Shear rates and normal stress levels were chosen to keep centrifugal effects small. The upper plate is free to move vertically, thus allowing for dilitation in the granular material. The outer wall is plexiglass lined with a removable sheet of clear polycarbonate. This allows for visual observations of the flow as well as measurement of the depth of motion. Thus the general shear response for granular media, as well as the dynamic yield criterion, can be studied over a range of conditions.

A series of laboratory experiments has been proposed to study the behavior of $\tan\phi_r$, the depth of motion, and the general shear response of granular-fluid media. To date, data has been collected for dry flows of spherical glass beads of densities $\rho_s$ = 2.47, 2.78, and 2.97 grams/cm$^3$ and diameters 1.1 mm and 1.85 mm. The data verifies the general Bagnoldian

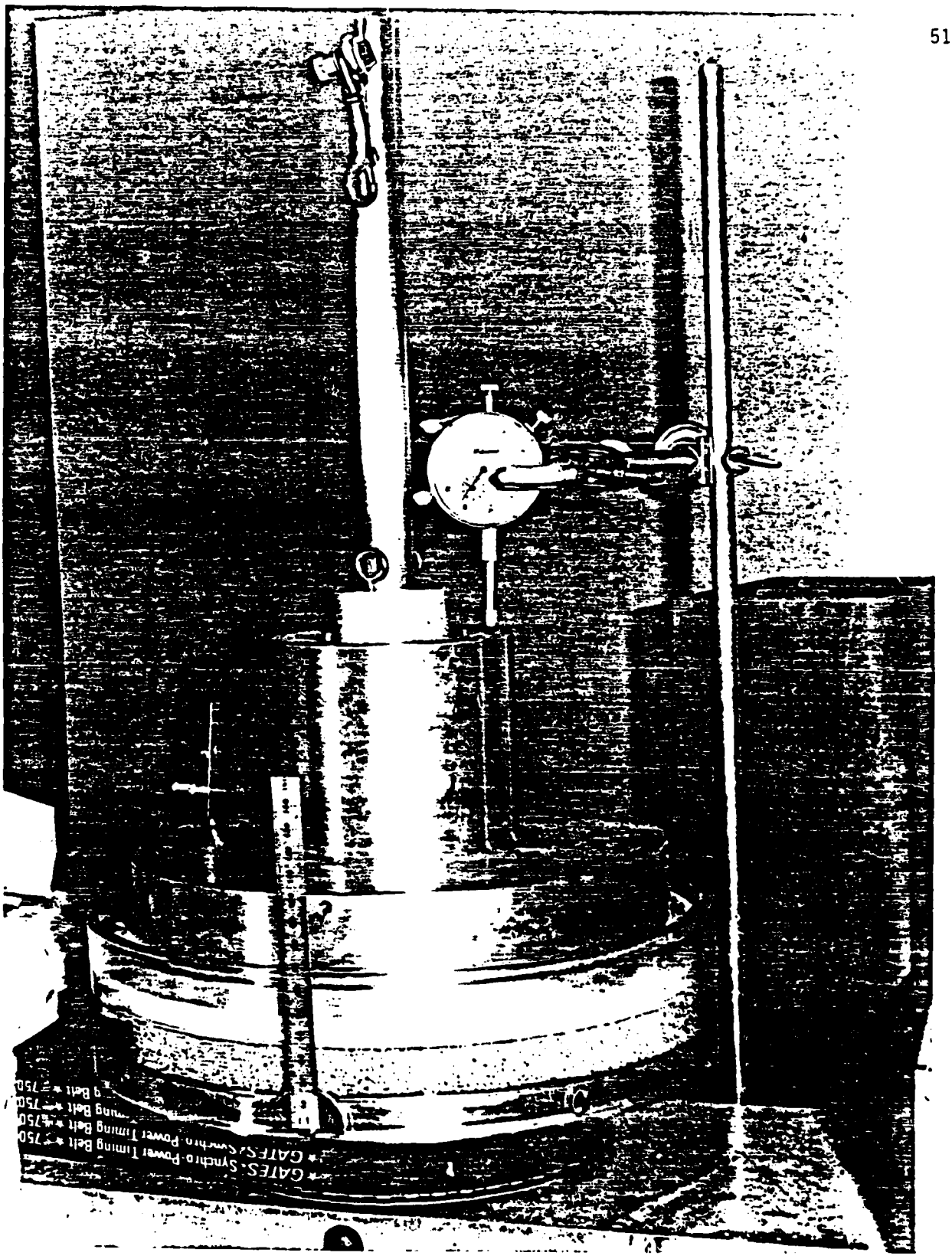

5.3

Figure B1-2. Annular shear cell to measure shear and normal stresses in granular fluid under traction.

81.90-2

concept that for fully mobilized shear flows at high shear rates, the shear stress is quatratic in shear rate, as seen in Figure B1-3. This behavior is quite different that that of a Newtonian fluid, for which shear stress is linear in shear rate. Cursory examination of the data indicates that under many conditions there can exist a shearing layer of grains on top of a nonshearing layer, as expected. For these considtions the parameter $\tan\phi_r$ varies within a narrow range, showing some dependence upon shear rate and granular concentration.

Following further analysis of this data a similiar series of experiments will be run using water as an interstitial fluid. Both wet and dry experiments will also be performed on quartz sand from a natural beach.

We are hopeful that these experiments will result in the ability to accurately predict the magnitude of the bedload. Furthermore, we think the data will prove quite valuable in the verification of the equations of motion for granular-fluid media. Once these equations and the appropriate boundary conditions are verified, a momentum based model for bedload sediment transport may be formulated.

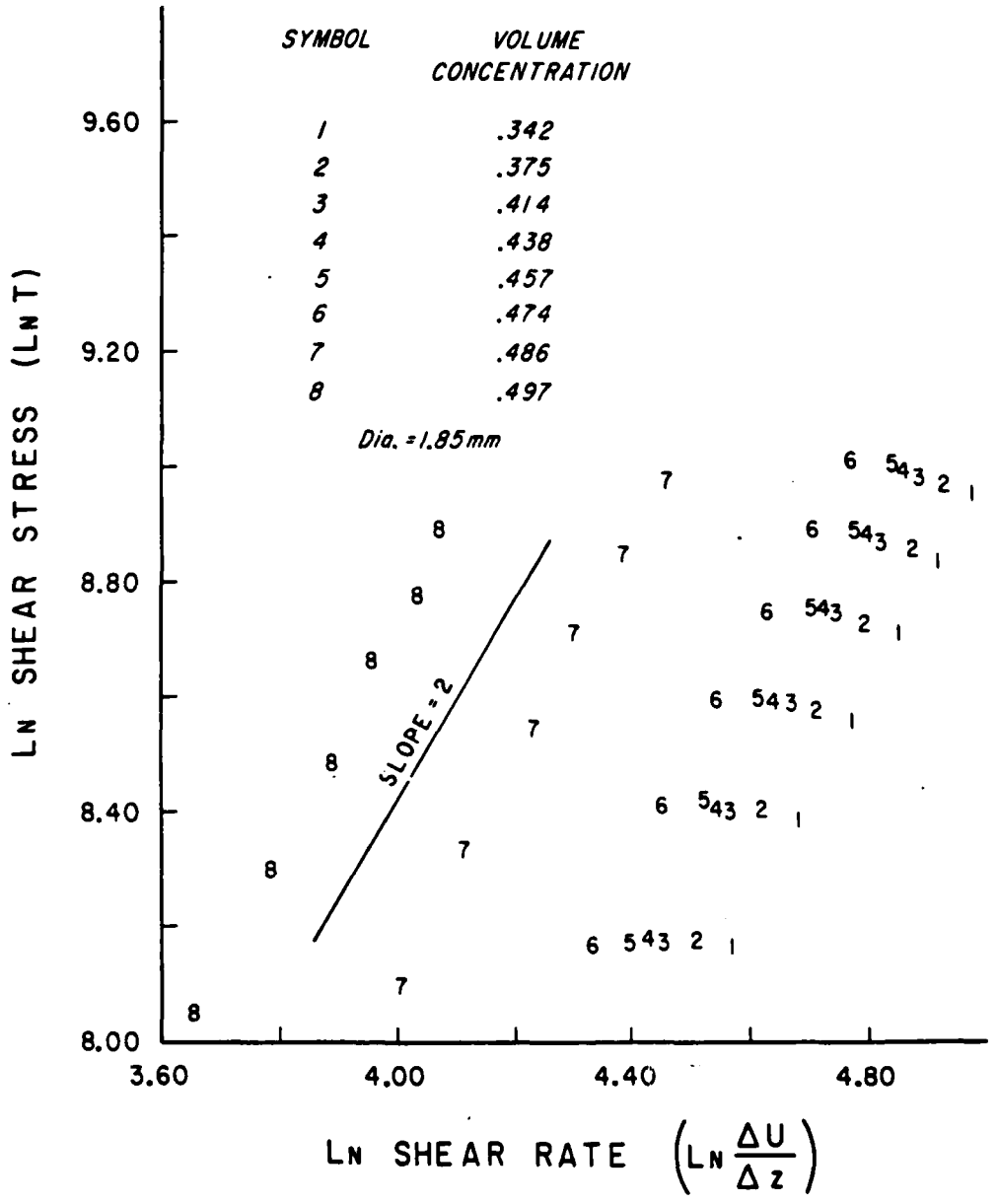


Figure B1-3. Shear stress vs shear rate for fully developed granular shear flow of spherical glass beads of diameter 1.85 mm. Numbers represent different volume concentrations. Note that scales are logarithmic, and data falls approximately on a line of slope 2 showing that the shear stress is quadratic in shear note.

B2. On-Offshore Transport of Sand (T. E. White and D. L. Inman)

The goal of this study is the prediction of on-offshore transport and the slopes of beach profiles from forcing functions, particularly waves and currents. This is a field study employing tracer techniques and bedload sensors (such as that being developed in Task B1.3) to measure sand movement, and wave arrays and current meters to measure the forcing functions.

Previous ONR-sponsored work (e.g. Winant et al 1975; Aubrey et al 1980) focused on the statistical description of beach profiles, and in a qualitative sense, related profile changes to physical forcing functions via empirical eigenfunction analysis. The present study is a more direct, mechanical approach to measuring the short-term (minutes to hours) bed response. Testing of state-of-the-art transport models such as that of Bailard and Inman (1981) then becomes possible since variables such as tracer layer thicknesses and currents that appear in the models can be measured directly.

An energetics model seeks an integral property, the total transport, by considering the energy flux and the rate of working for the entire sample grid. These energy fluxes and rates of working are, in turn, integral properties that reflect the fluid-granular particle dynamics and kinematics summed over the sampling grid. Since the property we seek, i.e. sediment transport rate, is an integrated property, conceptually and methodologically it makes good sense to use energetic models.

Energetics models relate local sediment transport rates, $\vec{i}$, to local fluid velocities, $\vec{u}$, through coefficients of efficiency, $\epsilon$, and friction, $c_f$. An energetics bedload model was developed by Bailard

and Inman (1981) based on a modification of Bagnold's (1963) steady stream-transport model, that allows for varying strengths of longshore currents and varying incident wave angles. The Bailard and Inman model predicts local bedload transport as:

$$\langle \vec{i} \rangle = \rho \frac{c_f \, \varepsilon_b}{\tan\phi} \left[ \langle |\vec{u}_t|^2 \vec{u}_t \rangle - \frac{\tan\beta}{\tan\phi} \langle |\vec{u}_t|^3 \rangle \vec{n}_x \right]$$

where $\langle\ \rangle$ means time-averaged, $\rho$ is the fluid density, $c_f$ is the fluid drag coefficient, $\varepsilon_b$ is the efficiency of bedload transport, $\tan\phi$ is the coefficient of granular friction, $\beta$ is the local bed slope in the negative x-direction, $\vec{n}_x$ is unit vector in the x-direction (positive onshore) and $\vec{u}_t$ is the time-varying velocity vector composed of the steady current $\bar{u}$ and the oscillatory current $\tilde{u}$.

In addition to bedload, a total load transport model requires a suspended load component. An energetics model for suspended load is being developed along the concepts of Bagnold (1963). However, differences between Bagnold's unidirectional stream transport and that under oscillatory waves introduces important modifications, making such a model more tentative than the bedload model for which there is now considerable body of support (e.g, Inman and Bowen, 1963; Inman, Komar and Bowen, 1968; Komar and Inman, 1970; Bailard and Inman, 1979; etc.).

Advection-diffusion models consider the kinematics of individual particles, integrated over all space to obtain total transport. This integration is extremely sensitive to local near-bed concentrations, velocities, and the position of the bed itself, both in terms of moving and static layers. Thus there are discrete properties which have large

gradients near one of the limits of integration, namely the bed whose position is not fully known. Since we seek an integrated property, it is a more logical procedure to calculate it from other integrated properties, as is done in energetics models. Further, the near bed variabilities introduce large errors into the integration for the total sediment transport. The value of the advection-diffusion model, beyond the obvious advantage of an independent estimate of transport, is that it provides much greater detail about depositional geometry, and hence gives more insight into the mechanics of transport under different surf and near-surf conditions, and into the effects of bedforms such as ripples and cusps on the transport processes. A common diffusion-advection model is obtained by modifying the diffusion equation to include advective terms (e.g., Rance, 1963):

$$\frac{\partial M}{\partial t} = k_x \frac{\partial^2 M}{\partial x^2} + k_y \frac{\partial^2 M}{\partial y^2} + k_z \frac{\partial^2 M}{\partial z} + U(z) \frac{\partial M}{\partial x} + V(z) \frac{\partial M}{\partial y}$$

where $M$ is the mass concentration of tracer, $k_x$, $k_y$, $k_z$ are the diffusion coefficients in the two horizontal directions and vertical direction respectively, and $U(z)$ and $V(z)$ are the horizontal transport velocities which are a function of $z$.

It must be recognized that the advection rates in the above relation vary with distance above the bed, and cannot be integrated without this knowledge. Once the diffusion coefficients and the advections are determined the equation can be tested against the distribution of tracer determined experimentally.

In the fall of 1980, four experiments were performed outside the breakers at Torrey Pines Beach to obtain data with which to test these models. The principle elements of this experiment were current meters to measure the fluid velocity, core samples to measure sand tracer distribution, and reference rods to measure net sand level changes. The core samples were located in a spatial grid of 8-12 samples, and 7-10 of these sample sets were taken during each experiment. Each spatial sample set can be used to determine the transport rate during the time period between sampling of that set and the previous set. Furthermore, each series of samples taken at one location but at successive times yields a single temporal estimate of transport (Inman et al., 1980). thus 5 sets of 10 samples each yields 15 transport estimates. These estimates are obtained from the relation

$$\vec{i} = (\rho_s - \rho)\, g\, N_o Z_o \vec{U}$$

where $N_o$ is the "at rest" solids concentration, $Z_o$ is the thickness of the layer of motion (obtained from the vertical tracer profile in cores), and $U$ is the transport velocity, determined from the relation

$$\vec{U} = \frac{\Sigma_i (M_i \vec{x}_i)/t_i}{\Sigma_i M_i}$$

where $M$ is the mass concentration of tracer, and $\vec{x}$ is the vector distance.

Preliminary analysis of the data shows interesting differences between transport in surfzone-wide tracer experiments (e.g., Komar and Inman, 1970; Inman et al., 1980) and those estimates obtained from local

experiments several meters outside the surfzone. Outside the breakpoint, transport velocity, $\vec{U}$, is consistently of the order of cm per minute, averaging about 5 cm $min^{-1}$ for onshore transport and 2 cm $min^{-1}$ for longshore transport. By comparison, surfzone experiments show longshore transport velocities 30 to 60 times greater.

Thus, the assumption that longshore transport rates are much higher inside the surfzone than outside appears to be valid. But the offshore transports show that surfzone transport is not total transport and the prediction of beach profile changes requires knowledge of the offshore transport relations. Estimates of transport rates also require that $Z_o$, the thickness of the layer of motion be known. Various statistical estimators of $Z_o$, which use vertical tracer concentration profiles as the input, have been proposed (Crickmore, 1967; Inman et al., 1980; Kraus et al., 1981). For complicated concentration profiles, namely the ones obtained in surfzone experiments, the more accepted estimators vary among themselves by about 10-20%. However, in the local offshore experiments at Torrey Pines, concentration profiles generally exhibited abrupt vertical cutoff of tracer, thereby yielding unambiguous estimates of the thickness of the layer of motion. These thicknesses could often be measured in the core samples with a ruler, because of high tracer concentrations.

Another difference between the two types of experiments is revealed by the actual magnitude of the estimates of $Z_o$. Estimates from offshore experiments usually give thicknesses of 1-2 cm. Surfzone experiments sometimes yield thicknesses that often range up to 7-10 cm. We suggest that the difference in magnitude and variance of $Z_o$ across

the surfzone is related to the differences in bottom velocities under plumging waves, bores, and backwash vortices repsectively. Plunging breakers have intense downward motion near the bottom that scours the sand bed, as do the intense vortices in the backwash. In contrast the bores that traverse the surfzone produce a horizontal velocity and tangential stress much like a progressive wave. Accordingly the measured values of $Z_o$ are greatest near the breakpoint and in the swashzone and least in the central portion of the surfzone.

The sand tracer data has been analyzed, yielding the transport velocities $U$, and the thickness of the layer of motion $Z_o$, and the transport rate from their product. Once the velocity field of the water is obtained by analysis of the current meter data then all of the necessary variables will be available and transport model testing can proceed.

Also, additional field experiments are being conducted in conjunction with the study of oscillatory bursting described in Task B1.1. Finally, comparisons of the thickness of the moving layer obtained in Task B1.1, in the present Task B2, and with estimates based on the laboratory study of rheology (Task B1.2) will provide valuable control limits as well as considerable insight into the mechanics of fluid-granular interactions.

B3. Coastal Forms

Research has continued on this task, which was first outlined at the ONR Coastal Dynamics Conference, Panama City, Florida. The goal is the development of a classification criterion for coastal forms based on the nature of the fluid driving forces and the regime of the relative grain stress near the bed surface (Task 3.1). In this model, the nature of the fluid motion and the resulting fluid-granular interactions determine whether the bedform is of the "interactive" type, and free to grow in size as under unidirectional flow leading from ripples to dunes; or of the "forced" type where the bedform geometry is constrained by length scales in the fluid motion as in the case of oscillatory waves where the orbital displacement determines the wavelength of oscillatory ripples.

B3.1 Bedforms Produced by Fluid-Granular Interaction (D. L. Inman and S. A. Jenkins)

Observations continue to verify the generality of the genetic classification of bedforms into "interactive" and "forced" forms. The classification scheme is shown in Figure B3-1 and a summary of the concepts leading to the primary types of bedform follows.

Fluid-granular interactions generate two primary classes of bedforms. The first is a class whose scales are determined by strong feedback mechanisms between bed perturbations and fluid eddies The scales of these forms cascades upward from small to larger features as grains to ripples to dunes, somewhat analogous to the vortex pairing in a turbulent shear layer. Since the fluid forming the features is essentially unbounded by

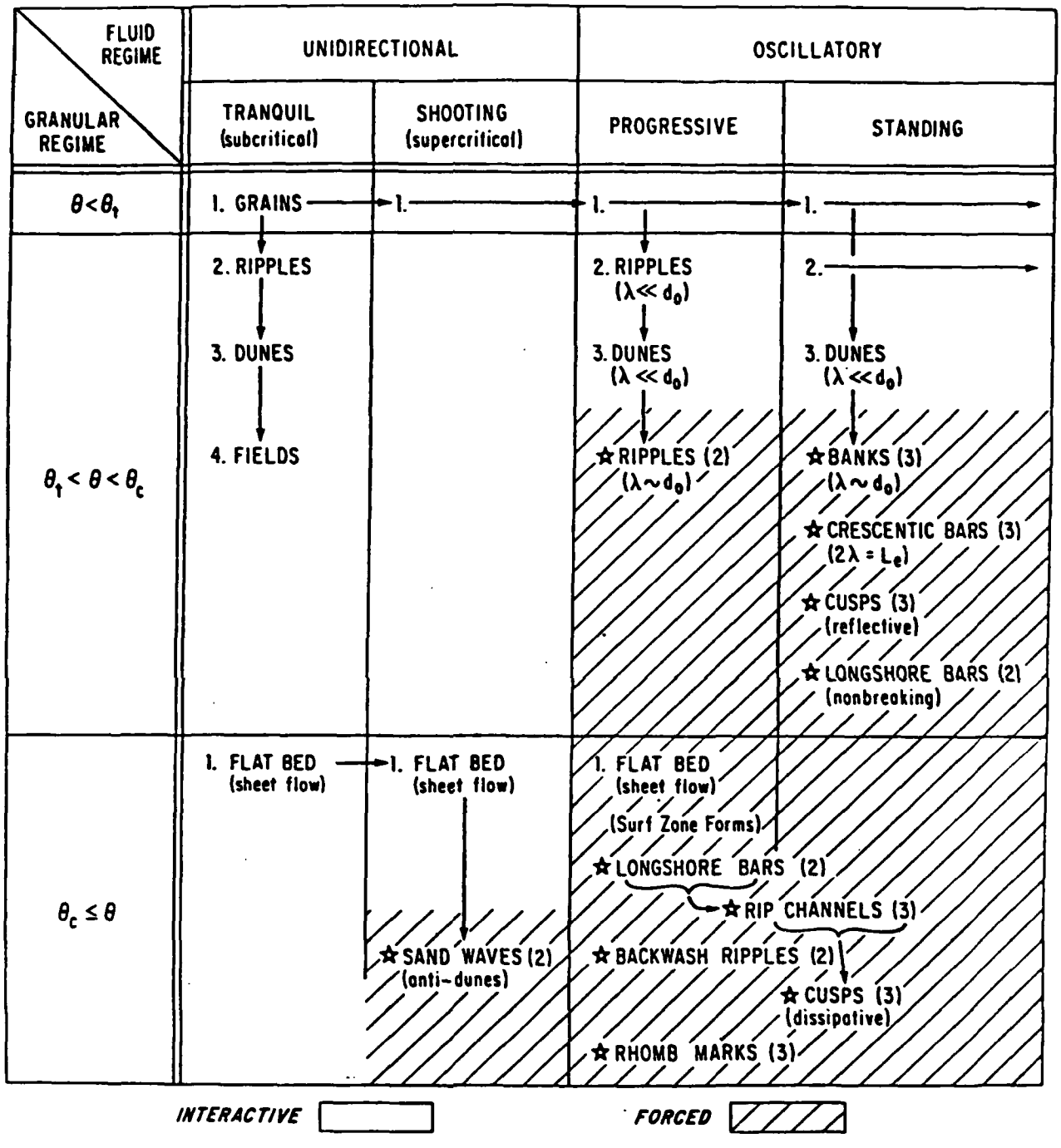


Figure B3-1. Classification of bed forms in terms of fluid motion and the relative grain stress. Numbers 1 through 4 indicate the roughness scales of "interactive" bed forms whose relative size depends primarily upon the upward cascade of eddy shedding perturbations of unconstrained fluid flow over an interactive bed. The asterisks * indicate "forced" forms whose scale and geometry are primarily controlled by the constraints imposed by the wave-like nature of the fluid motion; (2) and (3) following the form indicate two or three dimensionality of the form.

fluid constraints except at the bed where multiple scale interactions between the bed and the fluid occur, the bed features are referred to as "interactive forms". Typical interactive forms include ripples and dunes generated by the unidirectional flow of wind and water.

The scale and shape of the second class of bedforms are forced by exterior bounding constraints imposed upon the fluid, such as the wavelength of surface waves and the orbital diameters of fluid motions, and are referred to as "forced forms". Feedback in forced forms is initially absent and only occurs after the bed feature becomes well formed. Typical forced forms include wave-induced ripples, sand waves (anti-dunes), and beach features such as cusps, crescentic bars and backwash ripples. Although forced forms have no initial requirement of feedback from the bed to the fluid, feedback becomes progressively more intense as the bedform grows in amplitude. Eventually the bedform feedback becomes the limiting factor in determining the equalibrium amplitude of the bedform. The uniformity in heights of oscillatory vortex ripples and of beach cusps are examples of such controlling feedback.

The inertia accumulated in large scale bedforms sometimes results in their persisting long after the driving force that generated them has ceased. Obvious examples are longshore bars, rip channels, and beach cusps, which because of their great inertia may control the fluid motion for some time after the wave regime that formed them has changed. In these cases the features may be referred to as "remnant forced forms".

Beach cusps, a case where the amplitude of a forced form is limited by feedback is described in the following section.

B3.2 Cusps (R. T. Guza)

Beach cusps are crescentic shoreline features having pseudo-regular longshore wavelength ranging from a few centimeters to as much as several hundred meters. Cusp heights (horn to trough vertical distance) vary from a few centimeters to more than 2 meters. In the context of the bedform classification scheme discussed above, beach cusps are forced forms. The cusp wavelength is necessarily equal to half that of the edge wave responsible for cusp growth. Initial cusp growth is simply the sediment response to stresses arising from the longshore periodic flow field of the edge wave.

Progress has been made in investigating the feedback from cusps to edge waves which occurs when the cusp has grown to large amplitude. An equilibrium cusp amplitude is found such that the tendency of the incident waves to erase the beach cusps is balanced by the edge waves trying to increase the cusp amplitude. The theory, which uses the formalism of nonlinear triads, predicts that cusp heights depend on the mean beach slope and incident wave periods and amplitudes. The model prediction can also be cast into a form where the cusp amplitude depends only on the cusp wavelength, mean beach slope, and incident wave amplitude. In the most idealized case where the presence of cusps does not alter the mean beach slope from its value without cusps, and with strongly reflected incident waves, theory predicts

$$M_o = \frac{\pi}{2} \frac{a_T}{\lambda \beta} \leq 0.1$$

with $\beta$ the mean beach slope in radians, $\lambda$ the cusp wavelength and $a_T$ equal to half the cusp heights. $M_o$ defines a minensionless number which the theory suggests is the most important parameter in the problem. It turns out to be the ratio between the cusp steepness ($a_T/\lambda$) and the slope of the beach.

Note that the above equation predicts a maximum possible value for $M_o$, so that given the mean beach slope $\beta$ and cusp wavelength $\lambda$, all cusp amplitudes for which $M_o<0.1$ are possible. The theory is actually capable of predicting precise values for $M_o$, but this requires detailed information about the incident wave field which is not generally available.

To test the theoretical predictions observations of cusp amplitude $a_T$ were plotted versus $\lambda\beta$ (Figure B3-2). The data, which cover cusp amplitudes from a few centimeters to one meter, fall surprisingly close to the maximum value predicted by theory, $M_o = 0.1$. Although the theory makes many approximations and simplifications, the field data bears out that $M_o$ is indeed an important nondimensional number. Details of the theory and comparisons to field data are given in Guza and Bowen (1981).

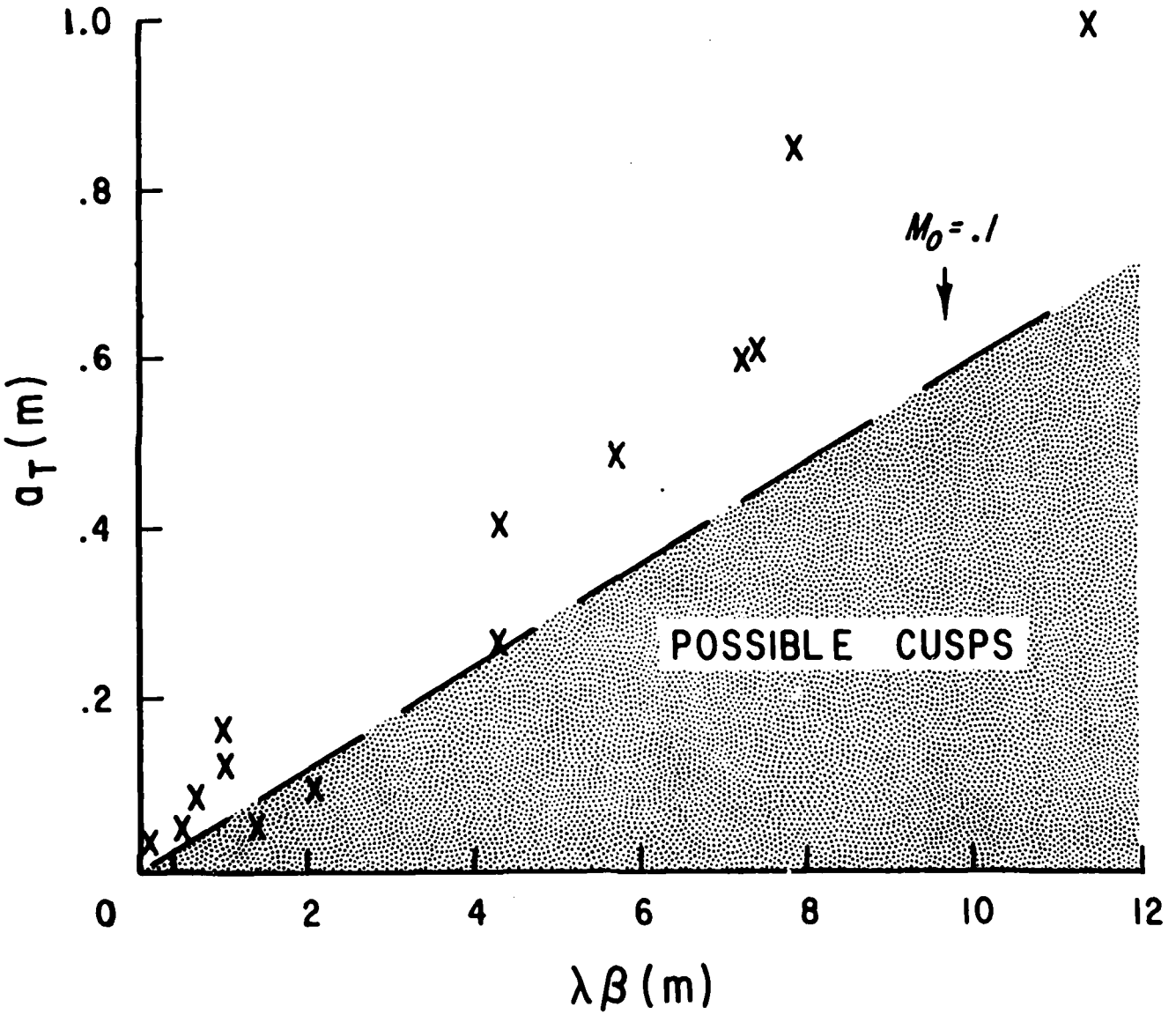


Figure B3-2. Field observations of cusp parameters compared with theory, $M_0 \leq 0.1$, where $M_0$ is the ratio of cusp steepness to beach slope.

B4. Shore Processes of Northern Adriatic Beaches (M. Weydert and D. L. Inman)

The long-term scientific objective of this cooperative project is to perform a detailed study of coastal bathymetry and shoreline changes in a shallow water region where wind waves, tidal Kelvin waves and local wind-generated circulation all are important driving forces. The study is in a setting where the historic shoreline changes are generally known since 800 B.C. and well known since the first century A.D. Much of our knowledge of historical changes results from the fact that the coastal city of Ravenna was the Adriatic Port for the Roman fleet since the first century A.D., so that the Roman Legion's Corps of Engineers made a number of harbor plans and conducted surveys of the coastline. Analysis of modern shoreline changes, with special emphasis on the sediment supply by rivers and the distribution of sediment along the coast by waves and currents will eventually yield a budget of sediment for the Emilia Romagna littoral cell.

As a first step toward defining the offshore wave climate in the northern Adriatic region, a wave and current array was installed on an AGIP gas production platform off the coast of Ravenna, Italy in July 1980. Fouling and damage (Figure B4-1) of the electromagnetic current meter was repaired in July 1981. The available data will be analyzed for gross frequency-directional spectra and spectral moments using methods discussed under Task A1. The wave data will be refracted into shore and used to predict the strength and direction of longshore currents.

Another method for predicting the wave climate and coastal currents is being implemented by our Italian counterparts. Cavalieri and Rizzoli (1977) have constructed a numerical wind-wave generation model

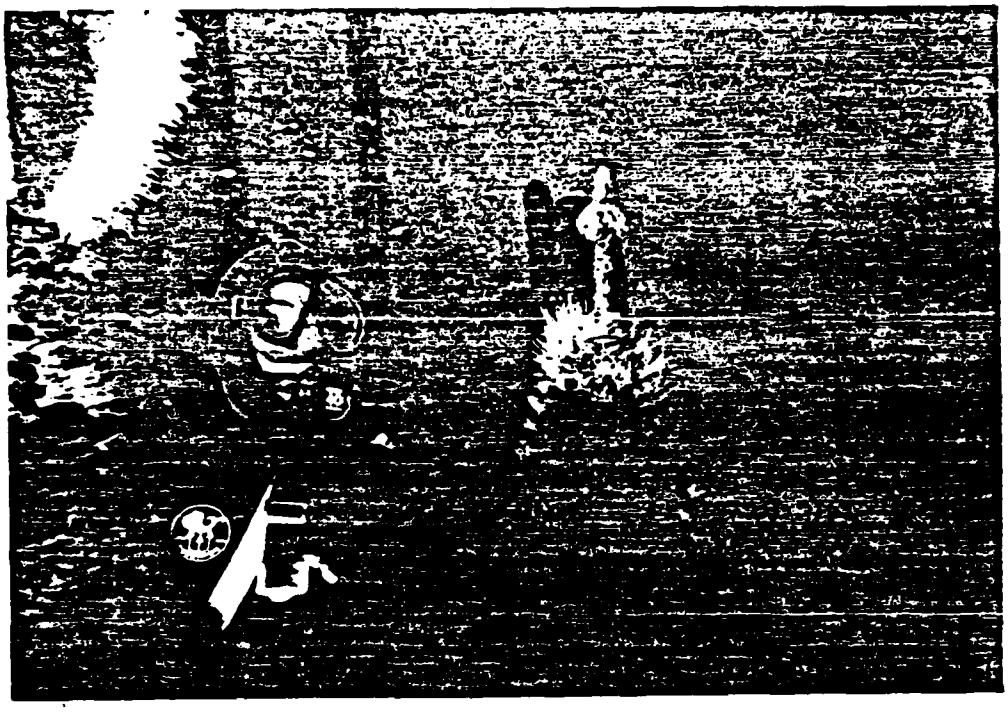

Figure B4-1. Underwater view of fouled electromagnetic current meter probe mounted to AGIP tower off Ravenna, Italy. Probe support is in fact broken, but being held in place by large mussel growth.

used to compute wave statistics, longshore currents (Figure B4-2) and other variables in the northern Adriatic from meteorological observations on the Italian and Yugoslavian coast. The model has been used to compute wave statistics furing the periods 11 to 18 July 1978 and 15 September to 16 October 1978. Work is underway to generate the model predictions during the time of actual wave measurements in 1980 and 1981 so that the two methods may be compared.

The wave and current measurements and predictions will also be used to estimate the dissipation and scattering of wave energy in this shallow sea. Definitive results in this area will depend upon the analysis of the data, currently under study.

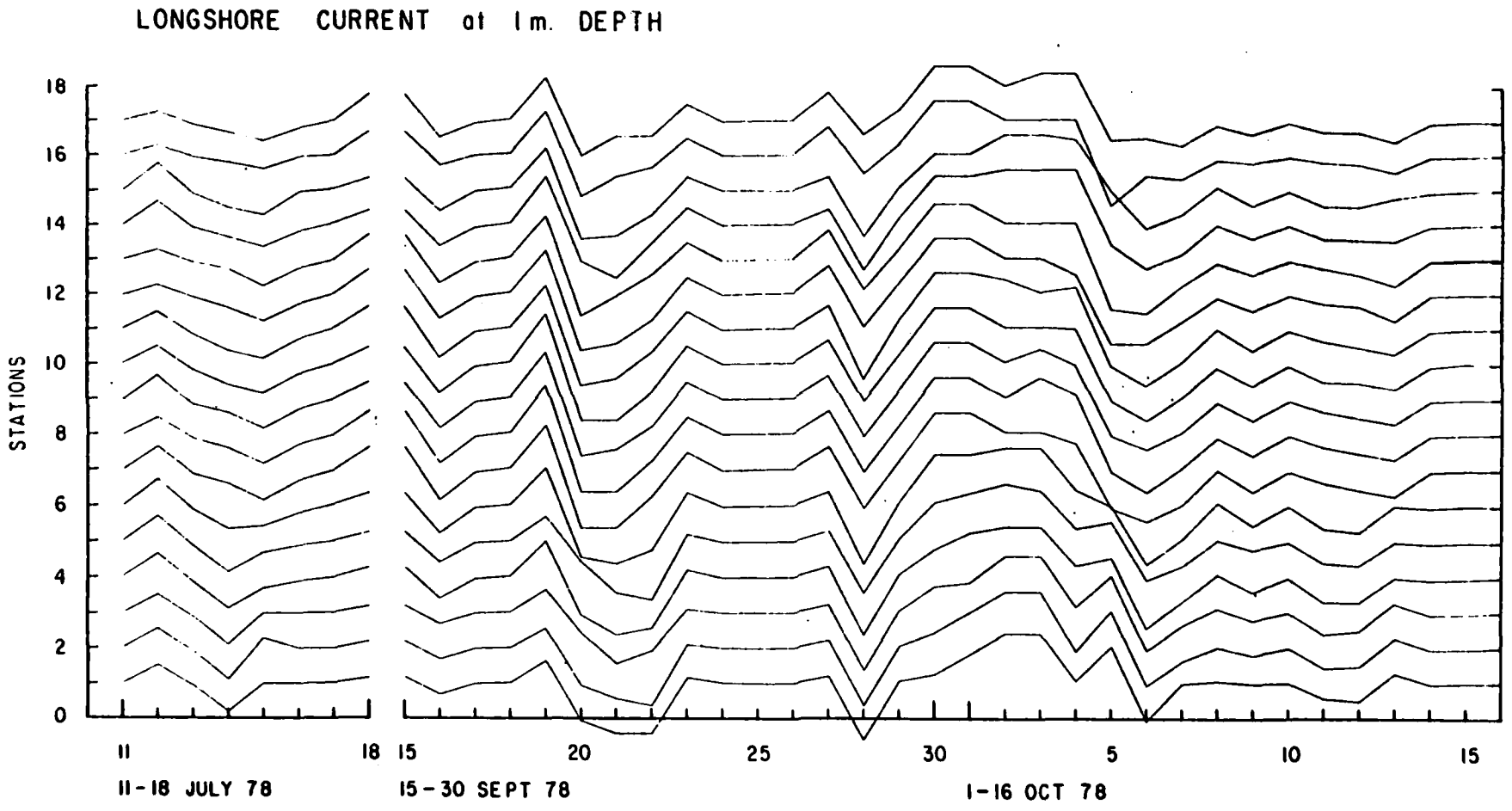


Figure B4-2. Longshore current prediction from wind-wave generation model. The spacing between each station number on vertical axis is current speed of 1 meter per sec. measured from a line drawn through the station number. Up is northerly current. Note the storm event 1-4 October 1978.

## C. COASTAL ZONE REMOTE SENSING

The objective of the remote sensing task is to use and refine existing techniques to study beaches and shelves, rather than to develop new remote sensing instrumentation. The opportunities for wide spatial coverage, without great time lags, of course makes remote sensing an attractive way of gathering data which would be prohibitively expensive to obtain using traditional "ground truth" sensors.

Task C1 addresses the advances made in SAR technology and suggests future development work necessary for oceanographically useful measurements. Task C2 summarizes the data manipulations performed on satellite infrared images of the California Current System and the processing being done to compare these images to current meter and drifter records.

C1. Remote Sensing of Waves (SAR) (S. S. Pawka)

In the past year, we have investigated the need for future developmental work on the measurement of wave frequency-directional spectra with synthetic aperture radar (SAR) systems. Remote sensing techniques for wave measurement were discussed extensively at the Workshop on Wave Measurement Technology, recently conducted by the National Academy of Sciences. The Shore Processes Laboratory was represented by Steve Pawka, an invited participant. Our input into the SAR discussions at the workshop drew heavily on our past experience with the comparison of L-band SAR and linear array data sampled at Torrey Pines Beach, described in detail in last year's progress report.

Several conclusions were drawn from the discussions on SAR systems: 1) Many advancements (e.g. image enhancement and processing techniques) have been made over the L-band technology used in the West Coast Experiment, 2) A majority of the ground truth experiments for SAR and other radar systems have been done with low directional resolution surface sensors (e.g. pitch/roll buoy) which do not adequately test the high resolution of the remote sensors, 3) SAR images show promise of accurate wave directional measurements but have an unknown transfer function which would enable the estimation of frequency spectra, 4) more ground truth verification of the SAR system is required.

The ideal location to stage a ground truth experiment is in the deep ocean, where the SAR measurements are made. This would eliminate the necessity to account for local shelf refraction effects in relating SAR measurements to shallow water ground truth. However, no practical high

resolution directional system has been developed for use on the surface in deep water. Ultimately, the most important use of the SAR system will be in the satellite sampling of intense wave activity in the deep ocean. Torrey Pines Beach is on a partially sheltered coast (see Progress A.2) and has relatively mild wind and wave conditions. It will not be certain whether testing in this location will be applicable to deep ocean storm conditions until the relationship between wave height and SAR image intensity (the transfer function) is better understood. Future ground truth experimentation at this site should be considered only after more developmental work is completed on th estimation of wave heights (frequency spectra) from SAR images. Therefore, no SAR/Torrey Pines ground truth experiments are planned for the immediate future.

Further developmental work on SAR systems may indicate the need for ground truth experiments in mild environmental conditions. Torrey Pines Beach would be a relatively desirable site for this experimentation. The local shelf is narrow and relatively plane. The directional accuracy of array measurements and refraction calculations at this site have been established at $1\text{-}2^{o}$ (deep water values). Additionally, a variety of complicated directional spectrum forms are persistent in the local wave climate.

An intense SAR sampling pattern in the area of the ground truth sensors is recommended. At least 10 independent realizations of the wave field on each sample day are required for reasonable comparison statistics. With a time lag of roughly 17 minutes between independent samples, this would require a minimum of 3 hours of sampling at a specific site. Also, variable heading flight paths should be employed to test the directional sensitivity of the SAR images. The sampling should span a period of about

20-30 days in February or March (season of high waves) to insure a variety of wave conditions at all wave frequencies. It is stressed that the utility of wave measurement systems for coastal science or engineering requires usable directional information in the frequency range 0.05-0.30 Hz.

C2. Remote Sensing of Shelf and Nearshore Dynamics (K. A. Kelly and C. D. Winant)

Collection and preliminary processing for a data set of infrared images in the California Current System from the NOAA-6 satellite is approximately two-thirds complete. Sorting through data for cloud-free areas has been unexpectedly time-consuming; however, recent software improvements at the SRSF have decreased the time required substantially. More than 120 images have been corrected for distortion, temperature-calibrated and mapped to a common projection. Sorting and mapping for the entire data set, a one-year time period, will be completed in the fall of 1981.

An empirical correction for the effects of moisture in a clear atmosphere, developed by Dr. Robert Bernstein, will be applied to the images after two filtering processes have been completed. The atmospheric correction algorithm requires the difference of apparent temperatures in bands 3 and 4 of the same image. Band 3 (13.7um) contains sensor noise equivalent to several tenths of a degree, while band 4 (11 um) is virtually noise-free. (See Figure C2-1A). The difference image contains information about the atmosphere and the sensor noise from band 3. (See Figure C2-1B). Data which are contaminated by clouds are apparent in this difference image as light areas. Note that the land, the Baja California coastline (right side of image), and Guadalupe Island (in the center of the image) are also visible in the difference.

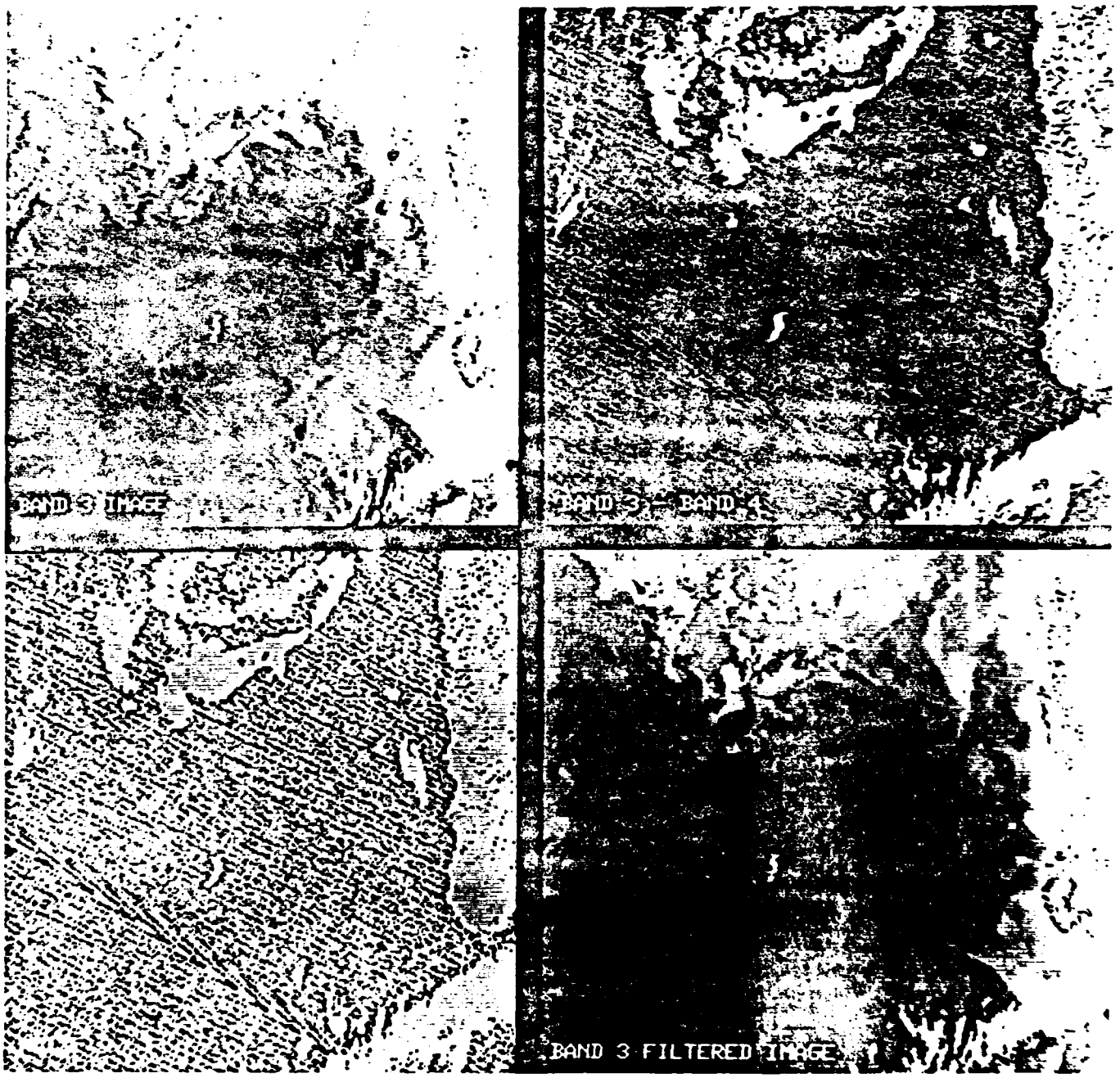


Figure C2-1. Removal of instrument noise from NOAA-6 image.

Two filters have been developed which use this difference image. The first filter isolates the noise from the AVHRR (See Figure C2.1C). The noise is subtracted from the original band 3 image to produce the smoothed version, shown in Figure C2-1D. Removing the noise in this way does not smooth ocean features, although it may blur somewhat the cloud edges. The second filter flags the cloudy areas. This filter is an adaptation of the method used by Coakley and Bretherton (in press) to determine cloud-cover statistics from the same data. Because the atmospheric correction is valid only for a clear atmosphere, data which are contaminated by clouds must be excluded from the statistical analysis. All of the processing procedures are nearly automatic because of the large amount of data. These filtering processes will be described in detail in a forthcoming paper.

Satellite data for the Coastal Ocean Dynamics Experiment (sponsored by NSF) area have been collected since April 1981. Preliminary analyses of doppler velocities and drifter tracks indicate unexpectedly energetic small scale motions. Satellite data will be useful in interpreting these surface velocity measurements. Images for the CODE area from late March through the end of June 1981 have been processed through the mapping step.

# 4. REFERENCES


Aubrey, D. G., D. L. Inman and C. D. Winant, 1980, "The statistical prediction of beach changes in Southern California," Jour. Geophys. Res., v 85, no C6, p 3264-3276.

Bagnold, R. A., 1954, "Experiments on a gravity-free dispersion of large solid spheres in a Newtonian fluid under shear," Proc. Roy. Soc. Series A, v 225, p 49-63.

Bagnold, R. A., 1963, "Mechanics of marine sedimentation," The Sea, v 3, M. N. Hill, ed., Wiley: New York, p 507-528.

Bailard, J. and D. L. Inman, 1979, "A reexamination of Bagnold's granular fluid model and bed load transport equation," Jour. Geophys. Res., v 84, p 7827-7833.

Bailard, J. A. and D. L. Inman, 1981, "An energetics bedload model for a plane sloping beach: local transport," Jour. Geophys. Res., v 86, n C3, p 2035-2043.

Bailard, J. and D. L. Inman, in prep., "An experimental study of two granular-fluid flows," to be submitted to Jour. Geophys. Res.

Bowen, A. J., 1969, "The generation of longshore currents on a plane beach," Jour. Marine Res., v 27, n 2, p 206-215.

Cavaleri, L. and P. Rizzoli, 1977, "Wind wave prediction in shallow water-theory and applications," Istituto per lo Studio della Dinamica delle Grandi Masse, Consiglio Nazionale delle Ricerche, Venice, Italy,

Coakley, J. A., Jr., and F. P. Bretherton, in press, "Cloud cover from high resolution scanner data: Detecting and allowing for partially filled fields of view," Jour. Geophys. Res.

Crickmore, M. J., 1967, "Measurement of sand transport in rivers with special reference to tracer methods," Sedimentology, v 8, p 175-228.

Dingler, J. R. and D. L. Inman, 1976, "Wave-formed ripples in nearshore sands," Proc. 15th Int. Conf. Coastal Eng., Amer. Soc. Civil Eng.

Flick, R. E. and M. D. Parker, 1980, "Geomagnetic induction to measure strong nearshore flow velocities," Oceans 80, Inst. Electrical and Electronics Eng., p 210-215.

Flick, R. E., R. T. Guza and D. L. Inman, 1981, "Elevation and velocity measurements of laboratory shoaling waves," Jour. Geophys. Res., v 86, n C5, p 4149-4160.

Goodman, N. R., 1957, "On the joint estimation of the spectra, cospectrum, and quadrature spectrum of a two-dimensional stationary gaussian process," Ph.D. Thesis, Scientific Paper No. 10, New York University, New York.

Guza, R. T. and A. J. Bowen, 1981, "On the amplitude of beach cusps," Jour. Geophys. Res., v 86, n C5, p 4125-4132.

Guza, R. T. and E. B. Thornton, 1981, "Wave set-up on a natural beach," Jour. Geophys. Res., v 86, n C5, p 4133-4137.

Guza, R. T. and E. B. Thornton, in press, "Swash oscillations on a natural beach," Jour. Geophys. Res.

Hasselman, K., W. H. Munk and G. MacDonald, 1963, "Bispectra of ocean waves," Time Series Analysis, M. Rosenblatt, ed., Wiley: New York, p 125-139.

Hinze, J. O., 1975, (2nd ed) Turbulence, McGraw-Hill, New York, 790 pp.

Inman, D. L., 1957, "Wave generated ripples in nearshore sands," Beach Erosion Board, Corps of Engineers, Tech Memo 100, 65 pp.

Inman, D. L., 1963, "Sediments: physical properties and mechanics of sedimentation," Chapter 5 of F. P. Shepard's Submarine Geology, Harper & Row Publ., p 101-147.

Inman, D. L. and R. A. Bagnold, 1963, "Littoral processes," The Sea, v 3, ed. M. N. Hill, Interscience Publ., p 529-553.

Inman, D. L. and A. J. Bowen, 1963, "Flume experiments on sand transport by waves and currents," Proc. 8th Int. Conf. Coastal Eng., Amer. Soc. Civil Eng., p 137-150.

Inman, D. L., P. D. Komar and A. J. Bowen, 1968, "Longshore transport of sand," Proc. 11th Conf. Coastal Eng., London, Amer. Soc. Civil Eng., v 1, p 298-306.

Inman, et al., 1980, "Field measurements of sand motion in the surf zone," Proc. 17th Conf. Coastal Eng., Amer. Soc. Civil Eng.

Jackson, R. G., 1976, "Sedimentological and fluid-dynamic implications of the turbulent bursting phenomenon in geophysical flows," Jour. Fluid Mech., v 77, p 531.

Komar, P. D. and D. L. Inman, 1970, "Longshore transport of sand," Jour. Geophys. Res., v 75, n 30, p 5914-5927.

Kraus, N. C., R. S. Farinato and K. Horikawa, in press, "An observation of nonsteady longshore sand transport in the surfzone," submitted to Jour. Geophys. Res.

Pawka, S. S., S. V. Hsiao, O. H. Shemdin and D. L. Inman, 1980, "Comparisons between wave directional spectra from SAR and pressure sensor arrays," Jour. Geophys. Res., v 85, n C9, p 4987-4995.

Pawka, S. S., in prep., "Wave directional characteristics on a partially sheltered coast," Ph.D. Dissertation, University of California, San Diego.

Rance, R. C., 1963, "The determination of quantities of sediment transport in oscillatory motion by consideration of the dispersion of tracer-sediment," Inter. Assoc. Hydraulic Res., 10th Congress, London, v 1, p 181-188.

Regier, L. A. , 1975, "Observations of the power and directional spectrum of oceanic surface waves," Ph.D. Dissertation, University of California, San Diego.

Savage, S. B., 1979, "Gravity flow of cohesionless granular materials in chutes and channels," Jour. Fluid Mech., v 92, part 1, p 53-96.

Schlichting, H., 1979, (seventh ed.) Boundary-Layer Theory, McGraw-Hill Book Co., New York, 817 pp.

Seymour, R. J. and A. L. Higgins, 1977, "A slope array for measuring wave direction," Proc. of a Workshop on Coastal Processes Instrumentation, La Jolla, CA., University of California, San Diego, Sea Grant Pub. No. 62, Institute of Marine Resources Ret.78-102, p 133-142.

Sleath, J. F.A., 1970, "Velocity measurements close to the bed in a wave tank," Jour. Fluid Mech., v 42, pt 1, p 111-123.

Winant, C. D., D. L. Inman and C. E. Nordstrom, 1975, "Description of seasonal beach changes using empirical eigenfunctions," Jour. Geophys. Res., v 80, n 15, p 1979-1986.

## 5. PUBLICATIONS 1980-1981


Aubrey, D. G., D. L. Inman and C. D. Winant, 1980, "The statistical prediction of beach changes in Southern California", Jour. Geophys. Res., vol 85, no C6, p 3264-3276.

Flick, R. E. and R. T. Guza, 1980, "Paddle generated waves in laboratory channels", Jour. Waterway Port Coastal & Ocean Div. WWI, p 79-97.

Flick, R. E., R. T. Guza and D. L. Inman, 1981, "Elevation and velocity measurements of laboratory shoaling waves", Jour. Geophys. Res., vol 86, no C5, p 4149-4160.

Flick, R. E. and M. D. Parker, 1980, "Geomagnetic induction to measure strong nearshore flow velocities", Oceans 80, Inst. Electrical and Electronics Eng., p 210-215.

Guza, R. T. and A. J. Bowen, 1981, "On the amplitude of beach cusps", Jour. Geophys. Res., vol 86, no C5, p 4125-4132.

Guza, R. T. and E. B. Thornton, 1980, "Local and shoaled comparisons of sea surface elevations, pressures, and velocities", Jour. Geophys. Res., vol 85, no C3, p 1524-1530.

Guza, R. T. and E. B. Thornton, 1981, "Wave set-up on a natural beach", Jour. Geophys. Res., vol 86, no C5, p 4133-4137.

Higgins, A. L., R. J. Seymour and S. S. Pawka, 1981, "A compact representation of ocean wave directionality", Applied Ocean Res., vol 3, no 3, p 105-112.

Inman, D. L., 1980, "Shore processes and marine archaeology (in China) ch 6, 47-65, in Oceanography in China, CSPRC Report, no 9, National Academy of Science, Washington, D.C.

Pawka, S. S., S. V. Hsiao, O. H. Shemdin and D. L. Inman, 1980, "Comparisons between wave directional spectra from SAR and pressure sensor arrays", Jour. Geophys. Res., vol 85, no C9, p 4987-4995.

## 6. DISTRIBUTION LIST

| | |
|---|---|
| Office of Naval Research<br>Coastal Sciences Program<br>Code 422CS<br>Arlington, VA 22217 | 3 copies |
| Defense Documentation Center<br>Cameron Station<br>Alexandria, VA 22314 | 12 copies |
| Director<br>Naval Research Laboratory<br>ATTN: Technical Information Officer<br>Washington, D.C. 20375 | 3 copies |
| Director<br>Office of Naval Research Branch Office<br>1030 East Green Street<br>Pasadena, CA 91101 | 1 copy |
| Commanding Officer<br>Office of Naval Research Eastern/ Central Regional Office<br>Building 114, Section D<br>666 Summer Street<br>Boston, MA 02210 | 1 copy |
| Office of Naval Research<br>Code 422PO<br>National Space Technology Laboratories<br>Bay St. Louis, MS 39529 | 1 copy |
| Office of Naval Research<br>Code 422PO<br>Washington, D.C. 22217 | 1 copy |
| Office of Naval Research<br>Code 100M<br>Washington, D.C. 22217 | 1 copy |
| Office of Naval Research<br>Operational Applications Division<br>Code 200<br>Arlington, VA 22217 | 1 copy |
| Commander<br>Naval Oceanographic Office<br>ATTN: Library, Code 1600<br>NSTL Station, MS 39529 | 1 copy |

Commander
Naval Coastal Systems Center
ATTN: Library, Code 116.1
Panama City, Florida 32401
1 copy

Librarian
Naval Intelligence
Support Center
4301 Suitland Road
Washington, D.C. 20390
1 copy

Officer in Charge
Environmental Prediction
Research Facility
Naval Post Graduate School
Monterey, CA 93940
1 copy

Director
Amphibious Warfare Board
U.S. Atlantic Fleet
Naval Amphibious Base
Norfolk, Little Creek, VA 23520
1 copy

Commander
Amphibious Force
U.S. Pacific Fleet
Force Meteorologist
Comphibpac Code 255
San Diego, CA 92155
1 copy

Commanding General
Marine Corps Development and
Educational Command
Quantico, VA 22134
1 copy

Chief of Naval Operations
OP 987J
Department of the Navy
Washington, D.C. 20350
1 copy

Commandant
U.S. Coast Guard
ATTN: GECV/61
Washington, D.C. 20591
1 copy

National Oceanographic Data Center (D764)
Environmental Data Services
NOAA
Washington, D.C. 20235
1 copy

Defense Intelligence Agency
Central Reference Division
Code RDS-3
Washington, D.C. 20301
1 copy

Central Intelligence Agency — 1 copy
ATTN: OCR/DD-Publications
Washington, D.C. 20505

Director — 1 copy
Coastal Engineering Research Center
U.S. Army Corps of Engineers
Kingman Building
Fort Belvior, VA 22060

Mr. Robert C. Beal
APL/Johns Hopkins University
Johns Hopkins Road
Laurel, MD 20810

Mr. Charles Bertram
Bertram Technology, Inc.
4 Maidstone Drive
Merrimack, NH 03054

Dr J. E. Breeding
Dept. of Oceanography & Ocean Engineering
Institute of Technology
Melbourne, FL 32901

Dr. Benno M. Brenninkmeyer
Boston College
Dept. of Geology & Geophysics
Boston, MA 02167

Dr. Davidson T. Chen
Naval Research Laboratory
Building 209
Washington, D.C. 20375

Dr. James M. Coleman, Director
Coastal Studies Institute
Louisiana State University
Baton Rouge, LA 70803

Dr. Will Connelly
U.S. Technology Corporation
Ft. Lauderdale, FL 33315

Dr. Thomas H. Dawson
United States Naval Academy
Department of Naval Systems Engineering
Annapolis, MD 21402

Prof. Klaus Hasselmann
Max-Planck Institute for Meteorology
Bundesstrasse 55, D-2000
Hamburg 13, Germany

Dr. G. D. Hickman
Applied Science Technology, Inc.
1011 Arlington Boulevard
Suite 137
Arlington, VA 22209

Dr. Edward E. Hindman II
Colorado State University
Department of Atmospheric Sciences
Fort Collins, CO 80523

Dr. Thomas H. Kinder
NORDA
NSTL Station, MS 29529

Dr. Paul D. Komar
Oregon State University
School of Oceanography
Corvallis, OR 97331

Dr. K. S. Krishnan
Systems Control, Inc.
1801 Page Mill Road
Palo Alto, CA 94304

Dr. Bruce M. Lake
TRW
One Space Park
Redondo Beach, CA 90278

Dr. Donald A. Leonard
Computer Genetics Corporations
4 Lakeside Office Park
Wakefield, MA 01880

Dr. Bruce S. Maccabee
Naval Surface Weapons Center
Dahlgren, VA 22448

Dr. John D. Milliman
Woods Hole Oceanographic Institution
Department of Geology & Geophysics
Woods Hole, MA 02543

Dr. Richard K. Moore
U. of Kansas Center for Research, Inc.
2291 Irving Hill Drive, Campus West
Lawrence, KS 66045

Dr. C. B. Officer
Dartmouth College
Department of Earth Sciences
Hanover, NH 03755

Dr. Thomas K. Poiker
Theodore D. Sterling Ltd.
Ste. 70, 1507 West 12th Avenue
Vancouver, British Columbia, Canada V6J 2E2

Dr. Phillip Shelley
EG&G Washington Analytical
Services Center, Inc.
2150 Fields Road
Rockville, MD 20850

Dr. Omar Shemdin
Jet Propulsion Laboratory
4300 Oak Grove Drive
Pasadena, CA 91103

Mr. Robert A. Shuchman
Environmental Research Institute
of Michigan, P.O. Box 8618
Ann Arbor, MI 48107

Dr. Choule Sonu
*Tekmarine, Inc.*
37 Auburn Avenue
Sierra Madre, CA 91024

Dr. W. Sturges
Florida State University
Department of Oceanography
Tallahassee, FL 32306

Dr. Joseph N. Suhayda
Louisiana State University
Civil Engineering Department
Baton Rouge, LA 70803

Prof. Thomas H. Vonder Haar
Colorado State University
Department of Atmospheric Sciences
Fort Collins, CO 80523

Dr. H. Wang
College of Engineering
University of Delaware
Newark, DE 19711

Mr. William T. Whelan
Telecommunications Enterprises
2430 Industrial Drive
Panama City, FL 32405

Dr. John A. Whitehead, Jr.
Woods Hole Oceanographic Institution
Department of Physical Oceanography
Woods Hole, MA 02543

Dr. L. D. Wright
University of Sydney, Coastal Studies Unit
Department of Geography
Sydney, NSW 2006, Australia


DAT
FILM